

# Eikonal waves, caustics and mode conversion in tokamak plasmas

A Jaun<sup>1,4</sup>, E R Tracy<sup>2</sup> and A N Kaufman<sup>3</sup>

<sup>1</sup> NADA, Royal Institute of Technology, 100 44 Stockholm, Sweden

<sup>2</sup> Department of Physics, College of William and Mary, Williamsburg, VA 23187-8795, USA

<sup>3</sup> Lawrence Berkeley National Laboratory and Physics Department, UC Berkeley, Berkeley, CA 94720, USA

E-mail: [jaun@kth.se](mailto:jaun@kth.se)

Received 24 July 2006, in final form 9 November 2006

Published 4 December 2006

Online at [stacks.iop.org/PPCF/49/43](http://stacks.iop.org/PPCF/49/43)

## Abstract

Ray optics is used to model the propagation of short electromagnetic plasma waves in toroidal geometry. The new RAYCON code evolves each ray independently in phase space, together with its amplitude, phase and focusing tensor to describe the transport of power along the ray. Particular emphasis is laid on caustics and mode conversion layers, where a linear phenomenon splits a single incoming ray into two. The complete mode conversion algorithm is described and tested for the first time, using the two space dimensions that are relevant in a tokamak. Applications are shown, using a cold plasma model to account for mode conversion at the ion-hybrid resonance in the Joint European Torus.

## 1. Introduction

The propagation of electromagnetic waves plays an important role for the operation of fusion energy devices, such as tokamaks and the International Thermonuclear Experimental Reactor (ITER). Typical applications include the heating of electrons and/or ions when the discharge is first initiated, tailoring the plasma current profile to access regimes with an improved confinement and detecting instabilities for plasma diagnostics under thermonuclear conditions.

A number of computational tools have been developed to capture the dielectric properties of a toroidal plasma, for waves propagating between the ion-cyclotron range of frequencies (ICRF, around 30 MHz) and the electron-cyclotron range of frequencies (ECRF, around 100 GHz). Depending on the ratio between the wavelength  $\lambda$  and a typical scale over which the plasma parameters vary  $L$ , two methods are commonly used to solve the Maxwell equations inside the plasma. Full wave codes (LION [1], ALCYON [2], TASK-WM [3],

<sup>4</sup> Author to whom any correspondence should be addressed.

PENN [4], TORIC [5], AORSA [6]) compute a discrete approximation of the integro-differential wave equations using a combination of finite differences, finite elements and/or fast Fourier transforms. Even if the formulation itself is general, practical solutions can only be obtained using the world's most powerful computers for cases with a limited number of wavelengths inside the computational domain  $\lambda/L \gtrsim 1$ . On the contrary, ray-tracing codes (TORAY [7], GENRAY [8], Brambilla and Cardinali's FW/LW code [9]) compute an eikonal approximation [10] of the wave equations using a system of ordinary differential equations in the limit  $\lambda/L \ll 1$ . Until recently, their application has however been limited by the presence of caustics (singular regions of the plasma where the field amplitude diverges due to a breakdown of the eikonal ansatz) and mode conversion layers (regions where both the frequency and the wave-vector of two modes coincide).

Linear mode conversion deserves particular attention. Indeed, the phenomenon can be used to deposit a large amount of ICRF power to generate non-inductive current away from the plasma centre. The combination of an intrinsically 2D toroidal geometry and the scale separation of fast (long wavelength) and slow waves (short wavelength that propagate at the same frequency) makes the full-wave modelling particularly difficult. Only a small number of scenarios have been reproduced so far for the ICRF [11–13]; realistic toroidal mode conversion calculations in the ECRF remain beyond the possibilities of the most powerful computers today. Even a dramatic increase of the computational resources in the coming decade will fall short of the formidable means that are required for an '*ab initio*' simulation of a discharge in ITER [14].

Recent developments in ray-based methods have opened the possibility of accounting for mode conversion in the ICRF [15] and could be extended further to the ECRF. Depending on the plasma parameters, ray-tracing methods are indeed much faster than full-wave calculations and give much-needed physical insight concerning the energy propagation. Ray-based methods are not meant to replace full-wave methods, but to complement them by allowing researchers to perform a wider range of parameter studies. Moreover, a significantly higher level of confidence in the modelling can be achieved if both the ray tracing and the full-wave computations give similar physical predictions.

This paper documents the development of the RAYCON code (for 'ray conversion'), which implements the first toroidal ray-tracing model that can tackle mode conversion between the fast magnetosonic (MS) and the ion-hybrid (IH) wave in the ICRF.

## 2. The RAYCON model

The relatively slow evolution of plasma equilibrium parameters (which occur with the radial diffusion of current inside the tokamak) is first separated from the much faster response induced by the perturbations from an electromagnetic wave.

A Soloviev equilibrium and parabolic profiles provide a simple analytic description directly within the code; they can easily be replaced by experimental values after interfacing with an equilibrium code. In the same spirit, a simple cold fluid plasma model is used in this paper to capture the essence of the mode conversion physics at the ion–ion hybrid resonance, but can later be extended to account for thermal effects and mode conversion to ion- or electron-Bernstein waves.

The RAYCON code has been implemented as a suite of MATLAB modules to provide for flexibility during the development and to develop a tool for graduate students to learn about RF heating.

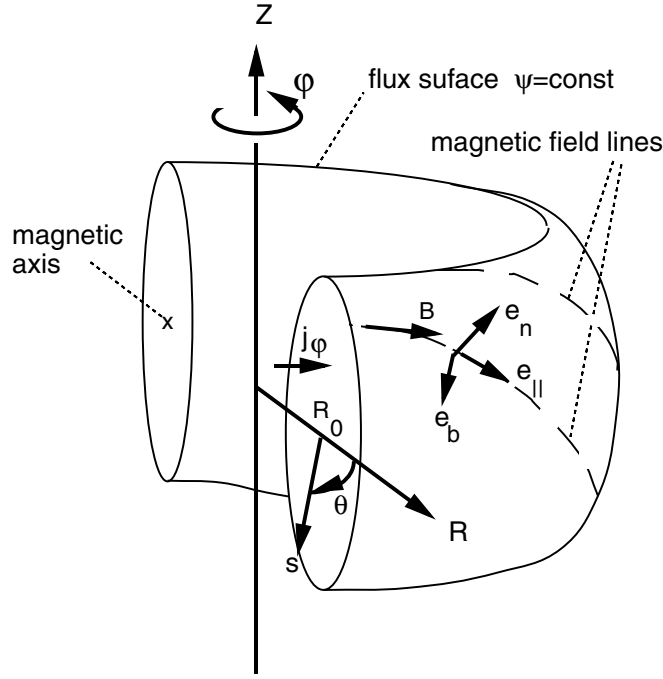


Figure 1. Toroidal geometry of the plasma in equilibrium.

### 2.1. Axisymmetric equilibrium with plasma current

A general description of a tokamak in equilibrium satisfies the nonlinear Grad–Shafranov equation and can only be solved numerically for an arbitrary plasma configuration. Particular solutions can however be obtained for a uniform toroidal magnetic flux  $T_0$  and a linear pressure profile  $p(\psi) = p_0(\psi_s - \psi)/\psi_s$  in the form of a Soloviev equilibrium in cylindrical coordinates  $(R, \varphi, Z)$  where the toroidal angle  $\varphi$  is ignorable

$$\psi(R, Z) = \frac{\psi_s}{a^2 R_0^2} \left( \frac{R^2 Z^2}{E^2} + \frac{1}{4} (R^2 - R_0^2)^2 \right). \quad (1)$$

The poloidal flux  $\psi$  describes concentric toroidal surfaces that surround the magnetic axis at  $(R = R_0; Z = 0)$  with an elongation  $E$ ; they are gradually deformed into a torus with an aspect ratio  $R_0/a$  on the outermost surface. The poloidal flux at the plasma boundary  $\psi_s$  depends on the amount of toroidal current and is related to the safety factor on the axis  $q_0 = T_0 a^2 E / (2\psi_s R_0)$ . The magnetic field on the plasma axis is entirely toroidal with a magnitude  $B_0 = T_0 / R_0$ . For simplicity, the species densities are modelled with parabolic functions

$$n(s) = n_0 (1 - cs^2)^d, \quad (2)$$

where the normalized radial variable  $s = \sqrt{\psi/\psi_s}$  is proportional to the square root of the poloidal magnetic flux. The model parameters  $c$  and  $d$  control the density at the plasma boundary and the peakedness of the density profile.

Defining toroidal coordinates  $(s, \theta, \varphi)$  with poloidal angle  $\theta = \arctan(Z/(R_0 - R))$ , the magnetic geometry in figure 1 can be described with the same set of coefficients that have

previously been used in the PENN code [4]:

$$R, Z, \frac{\partial s}{\partial R}, \frac{\partial s}{\partial Z}, \frac{\partial \theta}{\partial R}, \frac{\partial \theta}{\partial Z}, \frac{\partial^2 s}{\partial R^2}, \frac{\partial^2 s}{\partial R \partial Z}, \frac{\partial^2 s}{\partial Z^2}, \frac{\partial^2 \theta}{\partial R^2}, \frac{\partial^2 \theta}{\partial R \partial Z}, \frac{\partial^2 \theta}{\partial Z^2}. \quad (3)$$

Whether calculated analytically or input from an equilibrium code, the second order derivatives are sufficient to describe the ray trajectory alone; to compute the amplitude transport, they need to be supplemented by the third order derivatives that describe the magnetic field curvature

$$\frac{\partial^3 s}{\partial R^3}, \frac{\partial^3 s}{\partial R^2 \partial Z}, \frac{\partial^3 s}{\partial R \partial Z^2}, \frac{\partial^3 s}{\partial Z^3}. \quad (4)$$

Together with the density and the derivatives  $n_j(s)$ ,  $n'_j(s)$ ,  $n''_j(s)$  for each species labelled with an index  $j$ , the magnetic geometry (3)–(4) provides a complete description of the equilibrium in cylindrical coordinates. In particular, the static magnetic field vector is obtained from  $\mathbf{B} = \nabla\psi \times \nabla\varphi + T_0 \nabla\varphi$  and the magnetic field intensity  $B = \sqrt{|\nabla\psi|^2 + (T_0/R)^2}$ . Additional partial derivatives are calculated from projections in toroidal coordinates, for example using  $\nabla R \cdot (\nabla\theta \times \nabla\varphi) = (\partial_s R \nabla s + \partial_\theta R \nabla\theta + \partial_\varphi R \nabla\varphi) \cdot (\nabla\theta \times \nabla\varphi) = \nabla s \cdot (\nabla\theta \times \nabla\varphi) \partial_s R$  to calculate  $\partial_s R$ . From the magnetic field and the density in the tokamak, it is possible to calculate the cyclotron frequency  $\Omega_j = q_j B/m_j$  and the plasma frequency  $\omega_j = \sqrt{n_j q^2/\epsilon_0 m_j}$  of a species having mass  $m_j$  and charge  $q_j$ .

## 2.2. Plasma model and the polarization of electromagnetic waves

Combining Ampère and Faraday's law for an electromagnetic perturbation of the form  $\mathbf{E}(\mathbf{x}, t) = \mathbf{E}(\mathbf{x}) \exp(i[\Theta(\mathbf{x}) - \omega t])$  yields the wave equation

$$N^2 \mathbf{E} - \mathbf{N}(\mathbf{N} \cdot \mathbf{E}) = \bar{\bar{\epsilon}} \cdot \mathbf{E}, \quad (5)$$

where the wave-vector  $\mathbf{k}(\mathbf{x}) = \nabla\Theta$  is allowed to vary in space and the index of refraction  $N(\mathbf{x}) = ck/\omega$  is measured with respect to the speed of light in vacuum  $c$ . Define local magnetic unit vectors ( $\hat{\mathbf{e}}_n = \nabla s/|\nabla s|$ ,  $\hat{\mathbf{e}}_b = \hat{\mathbf{e}}_\parallel \times \hat{\mathbf{e}}_n$ ,  $\hat{\mathbf{e}}_\parallel = \mathbf{B}/B$ ) to separate the fast dynamic response of the species along the magnetic field from the one across. This produces a system with the dispersion tensor  $\bar{\bar{\mathbf{H}}}(\mathbf{x}, \mathbf{k}(\mathbf{x}))$

$$\bar{\bar{\mathbf{H}}}(\mathbf{x}, \mathbf{k}(\mathbf{x})) \cdot \mathbf{E}(\mathbf{x}) \equiv \begin{pmatrix} N_b^2 + N_\parallel^2 - \epsilon_{nn} & -N_n N_b - \epsilon_{nb} & -N_n N_\parallel - \epsilon_{n\parallel} \\ -N_n N_b - \epsilon_{bn} & N_n^2 + N_\parallel^2 - \epsilon_{bb} & -N_b N_\parallel - \epsilon_{b\parallel} \\ -N_n N_\parallel - \epsilon_{\parallel n} & -N_b N_\parallel - \epsilon_{\parallel b} & N_n^2 + N_b^2 - \epsilon_{\parallel\parallel} \end{pmatrix} \cdot \begin{pmatrix} E_n \\ E_b \\ E_\parallel \end{pmatrix} = 0, \quad (6)$$

where the plasma properties enter via the dielectric tensor  $\bar{\bar{\epsilon}}(\mathbf{x})$  and depend on the model. Choosing a cold fluid plasma, the dielectric tensor takes the form introduced by Stix [16]

$$\bar{\bar{\epsilon}} = \begin{pmatrix} S & iD & 0 \\ -iD & S & 0 \\ 0 & 0 & P \end{pmatrix}, \quad (7)$$

$$S = 1 + \sum_j \frac{\omega_j^2}{\Omega_j^2 - \omega^2}, \quad D = \sum_j \frac{\Omega_j}{\omega} \frac{\omega_j^2}{\Omega_j^2 - \omega^2}, \quad P = 1 - \sum_j \frac{\omega_j^2}{\omega^2}. \quad (8)$$

The  $3 \times 3$  cold fluid model can be further simplified by neglecting the electric field component parallel to the static magnetic field  $E_\parallel = 0$  while keeping only the upper  $2 \times 2$  set of components of the dispersion tensor (6).

More sophisticated models can in principle also be used provided that the dispersion tensor is Hermitian and non-degenerate with a rank  $M$ . Because the dispersion matrix  $\bar{\bar{H}}(\mathbf{x}, \mathbf{k})$  is Hermitian, its eigenvalues  $H_j(\mathbf{x}, \mathbf{k})$ ,  $j = 1, \dots, M$ , are real functions and its eigenvectors are orthogonal  $\hat{\mathbf{e}}_j^\dagger(\mathbf{x}, \mathbf{k}) \cdot \hat{\mathbf{e}}_{j'}(\mathbf{x}, \mathbf{k}) = \delta_{jj'}$ . Adopt the convention that the eigenvalues and eigenvectors have Roman indices and choose the notation  $H_j$  since the eigenvalues will play the role of ray Hamiltonians. Starting from the eigenvalue equation

$$\bar{\bar{H}}(\mathbf{x}, \mathbf{k}) \cdot \hat{\mathbf{e}}_j(\mathbf{x}, \mathbf{k}) = H_j(\mathbf{x}, \mathbf{k}) \hat{\mathbf{e}}_j(\mathbf{x}, \mathbf{k}), \quad j = 1, \dots, M, \quad \forall(\mathbf{x}, \mathbf{k}) \quad (9)$$

the dispersion matrix is first decomposed using the eigenvectors as a basis

$$\bar{\bar{H}}(\mathbf{x}, \mathbf{k}) = \sum_{j=1}^M H_j(\mathbf{x}, \mathbf{k}) \hat{\mathbf{e}}_j(\mathbf{x}, \mathbf{k}) \hat{\mathbf{e}}_j^\dagger(\mathbf{x}, \mathbf{k}). \quad (10)$$

Restricting these general expressions to the two-dimensional surface (called a *Lagrange manifold* imbedded in four-dimensional phase space  $(R, Z, k_R, k_Z)$ , since  $k_\varphi$  is constant and  $\varphi$  is ignorable due to toroidal symmetry) that is defined by  $(\mathbf{x}, \mathbf{k}(\mathbf{x}))$  with  $\mathbf{k}(\mathbf{x}) \equiv \nabla\Theta(\mathbf{x})$ , this yields

$$\bar{\bar{H}}(\mathbf{x}, \mathbf{k}(\mathbf{x})) \cdot \hat{\mathbf{e}}_j(\mathbf{x}, \mathbf{k}(\mathbf{x})) = H_j(\mathbf{x}, \mathbf{k}(\mathbf{x})) \hat{\mathbf{e}}_j(\mathbf{x}, \mathbf{k}(\mathbf{x})), \quad j = 1, \dots, M, \quad (11)$$

$$\bar{\bar{H}}(\mathbf{x}, \mathbf{k}(\mathbf{x})) = \sum_{j=1}^M H_j(\mathbf{x}, \mathbf{k}(\mathbf{x})) \hat{\mathbf{e}}_j(\mathbf{x}, \mathbf{k}(\mathbf{x})) \hat{\mathbf{e}}_j^\dagger(\mathbf{x}, \mathbf{k}(\mathbf{x})). \quad (12)$$

The wave equation requires  $\bar{\bar{H}} \cdot \hat{\mathbf{e}} = 0$ , so that on this surface, the eigenvector  $\hat{\mathbf{e}}_1$  for the null eigenvalue  $H_1$  can be used as one member of a local polarization basis that brings  $\bar{\bar{H}}$  into diagonal form. To prepare the discussion in the following sections, simply note here that in a conversion region involving two different eigenvalues  $(H_1, H_2)$ , the polarization vectors  $(\hat{\mathbf{e}}_1, \hat{\mathbf{e}}_2)$  change rapidly and are unstable to small perturbations in the definition of  $\bar{\bar{H}}$ . Hence, it will be necessary to find a more suitable basis that has nicer properties. These will be the ‘uncoupled’ polarizations  $(\hat{\mathbf{e}}_\alpha, \hat{\mathbf{e}}_\beta)$ : they are well behaved under small changes in  $\bar{\bar{H}}$  and connect smoothly onto  $(\hat{\mathbf{e}}_1, \hat{\mathbf{e}}_2)$  in a region where the ray will be matched with a local solution.

We now limit ourselves to the  $2 \times 2$  cold plasma model with  $M = 2$  eigenvalues and construct solutions using eikonal (WKB) methods. The next section provides a self-contained, albeit brief, summary of a methodology that is by now well established in other fields; it is included for completeness and also to introduce definitions and concepts we build upon later.

### 2.3. Eikonal equations

We follow Kaufman’s general formulation that is applicable for vector waves [17]; check also our tutorial [18] and references therein. In a weakly nonuniform medium, the phase factor  $\exp(i\Theta(\mathbf{x}))$  often varies more quickly than both the (real positive) scalar amplitude  $E(\mathbf{x})$  and the (complex) polarization vector  $\hat{\mathbf{e}}(\mathbf{x})$  of the electric field. Far from conversion regions and caustics, this makes the eikonal form

$$\mathbf{E}(\mathbf{x}, t) = \hat{\mathbf{E}}(\mathbf{x}) \exp(i[\Theta(\mathbf{x}) - \omega t]) \quad (13)$$

a good ansatz for solutions of the wave equation. The hat indicates a slow variation in  $\mathbf{x}$ .  $k_\varphi$  and  $\omega$  are fixed and suppressed to simplify the notation. For the same reason, the  $\perp$  subscript on  $\mathbf{k}$  and the associated gradient are also dropped. Insert equation (13) into the variational

principle and ignore the gradient acting on the slowly varying amplitude

$$\mathcal{A}[E] = \int dx E^* \cdot \bar{\bar{H}}(\mathbf{x}, \mathbf{k} = -i\nabla) \cdot E \Rightarrow \hat{\mathcal{A}}[E] \equiv \int dx \hat{E}^*(\mathbf{x}) \cdot \bar{\bar{H}}(\mathbf{x}, \mathbf{k} = \nabla\Theta(\mathbf{x})) \cdot \hat{E}(\mathbf{x}). \quad (14)$$

Because the action functional  $\hat{\mathcal{A}}[E]$  is invariant under a global shift of phase  $\Theta(\mathbf{x}) \rightarrow \Theta(\mathbf{x}) + \Theta_0$ , Noether's theorem implies that there is an associated conserved quantity, which is the wave action flux density  $\mathbf{J}(\mathbf{x})$ . Stationarity under variation of the phase  $\delta\Theta(\mathbf{x})$  gives  $\nabla \cdot \mathbf{J} = 0$ , where the action flux density is

$$\mathbf{J}(\mathbf{x}) = -[\nabla_k(\hat{E}^*(\mathbf{x}) \cdot \bar{\bar{H}}(\mathbf{x}, \mathbf{k}) \cdot \hat{E}(\mathbf{x}))]_{\mathbf{k}=\nabla\Theta(\mathbf{x})}. \quad (15)$$

Stationarity under the variation  $\delta\hat{E}$  gives

$$\bar{\bar{H}}(\mathbf{x}, \mathbf{k} = \nabla\Theta(\mathbf{x})) \cdot \hat{E}(\mathbf{x}) = 0. \quad (16)$$

Now choose a particular polarization, for example  $\hat{E}(\mathbf{x}) = E_1(\mathbf{x})\hat{e}_1(\mathbf{x}, \mathbf{k}(\mathbf{x}))$ . Because the eigenvectors of a hermitian matrix are orthogonal, the decomposition (12) implies the scalar equation

$$H_1(\mathbf{x}, \mathbf{k} = \nabla\Theta_1(\mathbf{x}))E_1(\mathbf{x}) = 0, \quad (17)$$

which, for nontrivial solutions, implies that

$$H_1(\mathbf{x}, \mathbf{k} = \nabla\Theta_1(\mathbf{x})) = 0. \quad (18)$$

This shows that the dispersion relation for the eikonal solution in channel 1 is simply obtained by setting the corresponding eigenvalue to zero. Note that it would have been possible to choose the polarization  $\hat{e}_2$ , leading to the condition similar to (17) and (18), but with  $H_2$ .

In the following section, the nonlinear partial differential equation (18) for the phase  $\Theta_1(\mathbf{x})$  will be solved by Hamilton's methods. This is generally possible to do locally, but usually not globally. The reason is that near caustics and in conversion regions the eikonal ansatz (13) breaks down. We will show later how to use asymptotic methods to match eikonal solutions across breakdown regions; for the present, we simply assume that the eikonal ansatz is valid and proceed to construct the corresponding solutions.

#### 2.4. Eikonal solution: ray trajectories

The eigenvalue  $H_1(\mathbf{x}, \mathbf{k}(\mathbf{x}))$  associated with the chosen polarization  $\hat{e}_1(\mathbf{x})$  plays the role of a ray Hamiltonian where space  $\mathbf{x}$  and the canonically conjugate coordinate, the wave-vector  $\mathbf{k}$ , have three toroidal components  $\mu \in \{R, \varphi, Z\}$ . In what follows, we adopt the notation  $\partial_\mu \equiv \partial/\partial x^\mu$ ,  $\partial^\nu \equiv \partial/\partial k_\nu$  and use Einstein's summation convention over repeated indices. Account for the spatial dependence of the wave-vector via the eikonal phase factor  $\mathbf{k}(\mathbf{x}(\sigma_1)) = \partial_\mu \Theta_1$  and apply Leibniz's chain rule to differentiate the eigenvalue  $H_1(\mathbf{x}, \nabla\Theta_1(\mathbf{x})) = 0$  with respect to  $x^\mu$

$$\partial_\mu H_1 + (\partial^\nu H_1)(\partial_{\mu\nu}\Theta_1) = 0. \quad (19)$$

This is true for all  $\mathbf{x}$  throughout the region where  $\Theta_1(\mathbf{x})$  is well defined. Now consider any smooth curve in this region  $\mathbf{x}(\sigma_1)$  parametrized by  $\sigma_1$ . The change in  $\mathbf{k}(\mathbf{x}(\sigma_1))$  along this curve is

$$\frac{dk_\mu}{d\sigma_1} = (\partial_{\mu\nu}\Theta_1) \frac{dx^\nu}{d\sigma_1}. \quad (20)$$

The particular choice  $dx^v/d\sigma_1 = -\partial^v H_1$  together with the identity (19) shows that  $dk_\mu/d\sigma_1$  satisfies  $dk_\mu/d\sigma_1 = +\partial_\mu H_1$ . Therefore, a wave that satisfies the dispersion relation (18) has rays that satisfy Hamilton's equations:

$$\frac{dx^v}{d\sigma_1} = -\partial^v H_1, \quad (21)$$

$$\frac{dk_\mu}{d\sigma_1} = +\partial_\mu H_1. \quad (22)$$

The ray parameter is related to the physical time via the relation

$$\frac{dt}{d\sigma_1} = \frac{\partial H_1}{\partial \omega}. \quad (23)$$

The system (21) and (22) can be written in a more compact form by introducing the notation  $\mathbf{z} \equiv (\mathbf{x}, \mathbf{k})$  for phase space coordinates and by defining the *Poisson bracket* of two functions

$$\{f, g\} = (\nabla_x f) \cdot (\nabla_k g) - (\nabla_k f) \cdot (\nabla_x g) \equiv \nabla_z f \cdot \bar{\mathbf{J}}_4 \cdot \nabla_z g, \quad (24)$$

where the  $4 \times 4$  symplectic matrix  $\bar{\mathbf{J}}_4$  is

$$\bar{\mathbf{J}}_4 = \begin{pmatrix} 0 & 0 & 1 & 0 \\ 0 & 0 & 0 & 1 \\ -1 & 0 & 0 & 0 \\ 0 & -1 & 0 & 0 \end{pmatrix}. \quad (25)$$

Using the Poisson bracket in phase space coordinates, Hamilton's equations can be written as

$$\frac{dz}{d\sigma_1} = \{H_1, \mathbf{z}\}. \quad (26)$$

A few words are in order here about the choice of the ray Hamiltonian, since it is possible to use either the determinant of the dispersion matrix  $\det(\bar{\mathbf{H}}) \equiv H = \prod_{j=1}^M H_j$  or one of its eigenvalues, e.g.  $H_1$ . Hamilton's equations imply that both describe the same trajectories but with a different parametrization of the ray. This comes from the product rule for the Poisson bracket, where  $dz/d\sigma = \{H_1 H_2, \mathbf{z}\} = H_1 \{H_2, \mathbf{z}\} + H_2 \{H_1, \mathbf{z}\}$ . On the surface  $H_1 = 0$ , this gives  $dz/d\sigma = H_2 \{H_1, \mathbf{z}\}$ , showing that the ray orbits are the same, but the parametrization has changed. The determinant has the advantage of being numerically efficient to compute, since it is polynomial in the entries of the dispersion matrix. It will be shown that it also contains the information to describe the most common 'avoided crossing' type of mode conversion, which has an associated saddle structure in phase space that is evident in the determinant but not in any eigenvalue treated separately. There are however several advantages to using an eigenvalue for the ray Hamiltonian, rather than using the determinant. For example, when a mode conversion region of an 'avoided crossing' type is approached, a second eigenvalue is getting small, so that the ray tends to 'slow down' and can numerically appear to come to a halt. The ray parametrization using an eigenvalue tends to be better behaved. In addition, the amplitude-transport equation in the next section is most easily derived from the action principle; this automatically leads to an expression for the action transport in terms of one of the eigenvalues, not the determinant.

### 2.5. Eikonal solution: amplitude, focusing tensor and phase

In multiple dimensions one must follow a family of rays in order to correctly account for the focusing and defocusing of rays that contributes to the amplitude transport. In the methodology of Kaufman [17], this is accomplished by transporting the *focusing tensor* of the eikonal phase

along each ray, hence implicitly carrying along information about neighbouring rays. While leading to an increase in the number of quantities that need to be computed for each ray, it reduces the total number that must be followed and should therefore be more efficient than following a large number of rays.

The action flux density (15) associated with  $H_1$  is conserved

$$\mathbf{J}_1(\mathbf{x}) = -E_1^2(\mathbf{x}) (\nabla_k H_1(\mathbf{x}, \mathbf{k}))|_k = \nabla \Theta_1(\mathbf{x}) \quad (27)$$

and can now be used to derive the amplitude-transport equation following the ray.

Set the divergence of equation (27) to zero and use (19) to obtain

$$0 = \partial_\mu (E_1^2 \partial^\mu H_1) = 2E_1 (\partial_\mu E_1) (\partial^\mu H_1) + E_1^2 \partial_\mu (\partial^\mu H_1) \quad (28)$$

$$= -E_1^2 \frac{d}{d\sigma_1} \ln E_1^2 + E_1^2 [(\partial_\mu^\mu H_1) + (\partial^{\mu\nu} H_1) (\partial_{\mu\nu} \Theta_1)]. \quad (29)$$

This yields an explicit expression for the transport of the amplitude  $E_1(\mathbf{x}) \equiv E(\mathbf{x}(\sigma_1))$

$$\frac{d}{d\sigma_1} \ln E_1^2(\mathbf{x}) = (\partial_\mu^\mu H_1) + (\partial^{\mu\nu} H_1) (\partial_{\mu\nu} \Theta_1). \quad (30)$$

The second derivative terms  $\partial_{\mu\nu} \Theta_1(\mathbf{x}) \equiv \partial_\mu k_\nu(\mathbf{x}(\sigma_1))$  are elements of the focusing/refraction tensor and account for the convergence and divergence of neighbouring rays. They satisfy their own evolution equations, which can be established by differentiating (19)

$$\partial_\lambda (\partial_\mu H_1) + \partial_\lambda [(\partial^\nu H_1) (\partial_{\mu\nu} \Theta_1)] = 0. \quad (31)$$

Now expand

$$\partial_{\lambda\mu} H_1 + (\partial_\mu^\rho H_1) (\partial_{\lambda\rho} \Theta_1) + [(\partial_\lambda^\nu H_1) + (\partial^{\nu\rho} H_1) (\partial_{\lambda\rho} \Theta_1)] (\partial_{\mu\nu} \Theta_1) = -(\partial_{\lambda\mu\nu} \Theta_1) (\partial^\nu H_1), \quad (32)$$

permute the indices  $\nu \leftrightarrow \lambda$  and substitute the left side into an expression for the evolution

$$\frac{d}{d\sigma_1} \left( \partial_{\nu\mu} \Theta_1(\mathbf{x}(\sigma_1)) \right) = (\partial_{\nu\mu\lambda} \Theta_1) \frac{dx^\lambda}{d\sigma_1} = -(\partial_{\nu\mu\lambda} \Theta_1) (\partial^\lambda H_1), \quad (33)$$

where the first Hamilton equation (21) has been used for the second equality. This yields an explicit expression for the evolution of the focusing/refraction tensor  $\nabla\nabla\Theta(\mathbf{x}(\sigma_1))$

$$\frac{d}{d\sigma_1} (\partial_{\mu\nu} \Theta_1(\mathbf{x})) = (\partial_{\mu\nu} H_1) + (\partial^{\lambda\rho} H_1) (\partial_{\mu\lambda} \Theta_1) (\partial_{\rho\nu} \Theta_1) + (\partial_\mu^\lambda H_1) (\partial_{\nu\lambda} \Theta_1) + (\partial_\nu^\lambda H_1) (\partial_{\mu\lambda} \Theta_1). \quad (34)$$

Now consider the evolution of the phase  $\Theta_1(\mathbf{x}) \equiv \Theta(\mathbf{x}(\sigma_1))$ . To lowest order in the eikonal parameter, this simply evolves according to

$$\frac{d}{d\sigma_1} \Theta_1(\mathbf{x}) = (\partial_\mu \Theta_1) \frac{dx^\mu}{d\sigma_1} = -k_\mu (\partial^\mu H_1). \quad (35)$$

There is also a phase associated with the polarization vector that must be transported along the ray. This is a higher order effect and its derivation is given in [19]. The polarization phase is determined from

$$\hat{\mathbf{e}}_1^* \cdot \frac{d\hat{\mathbf{e}}_1}{d\sigma_1} = -\frac{1}{2} H_{mn} \{e_{1n}, e_{1m}^*\}|_{k(\mathbf{x})}. \quad (36)$$

Here,  $H_{mn}$  are the elements of the dispersion tensor,  $\{ \}$  is the Poisson bracket (24) and  $e_{1n}$  is the  $n$ th component of the polarization vector  $\hat{\mathbf{e}}_1(\mathbf{x}, \mathbf{k})$  associated with mode '1'. The bracket must be evaluated using the polarization vector  $\hat{\mathbf{e}}_1(\mathbf{x}, \mathbf{k})$  as defined on phase space (not on  $x$ -space) and the result is evaluated at the point  $(\mathbf{x}(\sigma_1), \mathbf{k}(\mathbf{x}(\sigma_1)))$ .

The complete system of ordinary differential equations includes the four ray equations for the phase space coordinates  $(\mathbf{x}, \mathbf{k})$  (21,22), three transport equations for the  $2 \times 2$  symmetric

focusing tensor  $\nabla\nabla\Theta_1$  (34), one for the amplitude  $E_1$  (30), one for the phase  $\Theta_1$  (35) and the correction from the polarization phase (36). Note that four Hamilton equations (21)–(22) are sufficient to compute the trajectory of electromagnetic rays. The complete system with nine equations ((21), (22), (30), (34)–(36)) is however required to compute the propagation of electromagnetic power.

The eikonal approximation can break down, roughly speaking, in two different ways: by encountering a caustic or by encountering a mode conversion region. Both are discussed in the following sections. Before doing so, we quickly show how to define the initial conditions in order to launch the eikonal rays.

## 2.6. Initial conditions

To model the antenna located on the low field side (LFS) of the tokamak, rays with a chosen polarization  $\hat{e}_1(\mathbf{x})$  are launched from coordinates  $(R, Z)$  on a flux surface  $s = s_{\text{ant}}$  with an initial wave-vector that satisfy the dispersion relation  $H_1(R, Z, k_R, k_Z) = 0$ . The wavefront with an amplitude  $E_1$  and a phase  $\Theta_1$  is aligned with the magnetic flux surface, so that

$$\left. \frac{d^2\Theta_1}{dR^2} \right|_s dR^2 + 2 \left. \frac{d^2\Theta_1}{dRdZ} \right|_s dRdZ + \left. \frac{d^2\Theta_1}{dZ^2} \right|_s dZ^2 = 0. \quad (37)$$

Divide by  $dR^2$  and substitute the geometrical factor

$$\left. \frac{\partial Z}{\partial R} \right|_s = \frac{(\nabla s \times \nabla \varphi) \cdot \nabla Z}{(\nabla s \times \nabla \varphi) \cdot \nabla R} = - \frac{\partial s / \partial R}{\partial s / \partial Z} \quad (38)$$

to close the system with the toroidal components of  $\nabla H_1 = 0$

$$\frac{\partial^2\Theta_1}{\partial R^2} + 2 \frac{\partial^2\Theta_1}{\partial R\partial Z} \left( \frac{\partial Z}{\partial R} \right) + \frac{\partial^2\Theta_1}{\partial Z^2} \left( \frac{\partial Z}{\partial R} \right)^2 = 0, \quad (39)$$

$$\frac{dH_1}{dR} = \frac{\partial H_1}{\partial R} + \frac{\partial H_1}{\partial k_R} \frac{\partial^2\Theta_1}{\partial R^2} + \frac{\partial H_1}{\partial k_Z} \frac{\partial^2\Theta_1}{\partial R\partial Z} = 0, \quad (40)$$

$$\frac{dH_1}{dZ} = \frac{\partial H_1}{\partial Z} + \frac{\partial H_1}{\partial k_R} \frac{\partial^2\Theta_1}{\partial R\partial Z} + \frac{\partial H_1}{\partial k_Z} \frac{\partial^2\Theta_1}{\partial Z^2} = 0. \quad (41)$$

The solution of this linear system prescribes the focusing tensor ( $\partial_{\mu\nu}\Theta_1$ ) and the antenna phasing. It completes the 9 scalars that are required to start the integration with the initial vector

$$(R, Z, k_R, k_Z, \partial_{RR}\Theta_1, \partial_{RZ}\Theta_1, \partial_{ZZ}\Theta_1, \ln E_1^2, \Theta_1)^T. \quad (42)$$

The eikonal approximation we have been describing up to this point can break down locally in two different ways. Firstly by the development of caustics, where rays of the same mode form an envelope, and secondly by mode conversion, where rays associated with different modes can resonantly interact. These require two very different methods of approach, but both can be dealt with locally and lead to matched asymptotic methods for piecing together eikonal solutions across the breakdown regions.

## 2.7. Caustics

The focusing/refraction of neighbouring rays and their reflection at the plasma boundary can result in the crossing of rays in  $\mathbf{x}$ -space. This leads to arbitrarily large components of  $\nabla_x \nabla_x \Theta_1$  and unphysical singularities of the wave amplitude along the ray (30). (In this section only, the subscript on the gradient  $\nabla_x$  is used in order to distinguish it from the gradient in  $\mathbf{k}$ -space,  $\nabla_k$ .)

In the rest of the paper, all gradients are with respect to  $\mathbf{x}$ .) Near caustics, the eikonal approximation is no longer valid. A local solution must be found and matched to the incoming and outgoing rays. The basic ideas for dealing with caustics in multidimensions are due to Maslov and co-workers from the 1960s. They have now been developed to a very sophisticated level and incorporated into numerical algorithms. The use of these methods is now probably most advanced in the Atomic, Molecular and Optical Physics literature, where comparisons between ‘semi-classical’ methods and numerical solutions of Schrödinger’s equation have demonstrated their quantitative accuracy [20]. An example of the treatment for the most commonly occurring caustics is here presented in detail to illustrate the method and to show how it has been implemented in the RAYCON code.

Because Hamilton’s equations satisfy uniqueness, intersections can never occur in phase space. A wave can therefore always be transformed from  $x$ - to  $k$ -space to avoid singular amplitudes in the neighbourhood of caustics. Introduce the forward transformation

$$\tilde{\mathbf{E}}(\mathbf{k}) = \int d\mathbf{x} e^{-i\mathbf{k}\cdot\mathbf{x}} \mathbf{E}(\mathbf{x}) = \int d\mathbf{x} e^{i\psi(\mathbf{x},\mathbf{k})} E(\mathbf{x}) \hat{\mathbf{e}}(\mathbf{x}, \mathbf{k}(\mathbf{x})) \quad (43)$$

and evaluate (43) by the method of stationary phase with  $\psi(\mathbf{x}, \mathbf{k}) = \Theta_1(\mathbf{x}) - \mathbf{k} \cdot \mathbf{x}$ . For a given  $\mathbf{k}$ , the phase  $\psi$  is stationary with respect to  $\mathbf{x}$  at  $\mathbf{x}_0(\mathbf{k})$ , which is the inverse relation to  $\mathbf{k}(\mathbf{x})$

$$0 = \partial_\mu \psi = \partial_\mu \Theta_1 - k_\mu. \quad (44)$$

Taylor-expand  $\psi$  about the stationary point and truncate at the quadratic term:

$$\psi(\mathbf{x}, \mathbf{k}) = \psi(\mathbf{x}_0, \mathbf{k}) + \mathbf{X} \cdot \nabla_x \psi + \frac{1}{2} \mathbf{X} \mathbf{X} : \nabla_x \nabla_x \psi, \quad (45)$$

where  $\mathbf{X} = \mathbf{x} - \mathbf{x}_0$ . Now define the transformed eikonal phase as  $\tilde{\Theta}_1(\mathbf{k}) \equiv \psi(\mathbf{x}_0, \mathbf{k}) = \Theta_1(\mathbf{x}_0(\mathbf{k})) - \mathbf{k} \cdot \mathbf{x}_0(\mathbf{k})$  which, with the help of (44), gives  $\mathbf{x}_0(\mathbf{k}) = -\nabla_k \tilde{\Theta}_1$ . The Maslov transformation (43) becomes

$$\tilde{\mathbf{E}}(\mathbf{k}) = E(\mathbf{x}_0) \exp(i\tilde{\Theta}_1) \hat{\mathbf{e}}(\mathbf{x}_0, \mathbf{k}) \int_{-\infty}^{\infty} d\mathbf{X} \exp\left(\frac{1}{2} i \mathbf{X} \mathbf{X} : \nabla_x \nabla_x \Theta_1 |_{\mathbf{x}_0(\mathbf{k})}\right). \quad (46)$$

The factors outside the integration show that the wave is also eikonal in  $k$ -space. The remaining integral can be calculated analytically for (dim=2) toroidal space variables ( $R, Z$ ) using the identity  $\int_{-\infty}^{+\infty} ds \exp(\frac{1}{2} i \beta s^2) = (\sqrt{2\pi/|\beta|}) \exp(i\frac{\pi}{4} \text{sign}\beta)$  which gives

$$\int_{-\infty}^{\infty} d^{\text{dim}} X \exp\left(-\frac{1}{2} i \mathbf{X} \mathbf{X} : \nabla_x \nabla_x \Theta_1\right) = \frac{(2\pi)^{\text{dim}/2}}{\sqrt{|\det \nabla_x \nabla_x \Theta_1|}} \exp\left(-i\frac{\pi}{4} \sum_{j=1}^{\text{dim}} \text{sign}(\lambda_j)\right), \quad (47)$$

where  $\lambda_j$  are eigenvalues of  $\nabla_x \nabla_x \Theta_1$ . The solution (46) is the Fourier transform of an eikonal wave as it enters the caustic region and is easy to evaluate using a multiplication

$$\tilde{\mathbf{E}}(\mathbf{k}) = E(\mathbf{x}_0) \exp(i\tilde{\Theta}_1) \hat{\mathbf{e}}(\mathbf{x}_0, \mathbf{k}) \frac{2\pi}{\sqrt{|\det \nabla_x \nabla_x \Theta_1|}} \exp\left(-i\frac{\pi}{4} [\text{sign}(\lambda_1) + \text{sign}(\lambda_2)]\right). \quad (48)$$

The transformed focusing tensor  $\nabla_k \nabla_k \tilde{\Theta}_1$  is obtained first by substituting the definition  $(\partial_{\mu\nu} \Theta_1) = \partial k_\mu / \partial x^\nu$  and since  $(\partial k_\mu / \partial x^\beta)(\partial x^\beta / \partial k_\nu) = \delta_\nu^\mu$ , this yields  $\nabla_k \nabla_k \tilde{\Theta}_1 = -(\nabla_x \nabla_x \Theta_1)^{-1}$ .

After transformation, an eikonal solution is constructed in  $k$ -space, using methods analogous to those already described for  $x$ -space, until it is possible to transform back to  $x$ -space on the far side of the caustic and fit to an outgoing ray. Extending the amplitude

transport from section 2.5 to  $k$ -space, the transformed focusing tensor, amplitude and phase are found to evolve according to

$$\frac{d}{d\sigma_1}(\partial^{\mu\nu}\tilde{\Theta}_1(\mathbf{k})) = -(\partial^{\mu\nu}H_1) - (\partial_{\lambda\rho}H_1)(\partial^{\mu\lambda}\tilde{\Theta}_1)(\partial^{\rho\nu}\tilde{\Theta}_1) - (\partial_\lambda^\mu H_1)(\partial^{\nu\lambda}\tilde{\Theta}_1) - (\partial_\lambda^\nu H_1)(\partial^{\mu\lambda}\tilde{\Theta}_1), \quad (49)$$

$$\frac{d}{d\sigma_1} \ln \tilde{E}_1^2(\mathbf{k}) = -(\partial_\mu^\mu H_1) - (\partial_{\mu\nu}H_1)(\partial^{\mu\nu}\tilde{\Theta}_1), \quad (50)$$

$$\frac{d}{d\sigma_1}\tilde{\Theta}_1(\mathbf{k}) = -x^\nu(\partial_\nu H_1). \quad (51)$$

The backward Maslov transformation from  $k$ - to  $x$ -space can then be defined from the ray parameters evaluated at  $(\mathbf{x}, \mathbf{k}_0(\mathbf{x}))$  and yields

$$E(\mathbf{x}) = E(\mathbf{k}_0) \exp(i\Theta_1) \hat{\mathbf{e}}_1(\mathbf{x}, \mathbf{k}_0) \frac{(2\pi)^{-1}}{\sqrt{|\det \nabla_k \nabla_k \tilde{\Theta}_1|}} \exp\left(+i\frac{\pi}{4}[\text{sign}(\tilde{\lambda}_1) + \text{sign}(\tilde{\lambda}_2)]\right), \quad (52)$$

where  $\tilde{\lambda}_1, \tilde{\lambda}_2$  are the two eigenvalues of  $\nabla_k \nabla_k \tilde{\Theta}_1$ . This transformation is performed after having integrated across the caustic in  $x$ -space, before caustics can also be encountered in  $k$ -space when the components of  $\nabla_k \nabla_k \tilde{\Theta}_1$  become large.

The other manner in which the eikonal approximation breaks down is in a conversion region, which is the topic we now turn to.

## 2.8. Mode conversion

In a plasma composed of two ion species, the energy of a fast MS ray propagating from the LFS to the HFS of the tokamak is split among a transmitted MS ray, a reflected MS ray and a converted IH ray. The phenomenon occurs in the neighbourhood of the IH resonance where the wave frequency matches the IH frequency:  $\omega^2 = \Omega_{12}^2 \equiv (\omega_1^2 \Omega_2^2 + \omega_2^2 \Omega_1^2)/(\omega_1^2 + \omega_2^2)$ . Using the phase space description recently reviewed in [18], the most common type of mode conversion in toroidal geometry occurs in two steps as an ‘avoided crossing’ in phase space. More complex scenarios have been identified [21, 22] but are not considered in this work. Figure 2 suggests how an incoming MS ray launched from the LFS first encounters a resonance in  $x$ -space and is gradually transformed into a *converted* ray propagating mainly in  $k$ -space. A new MS ray is *transmitted* through an evanescent region and propagates further to the HFS in  $x$ -space. In a second step (not shown in the figure), the first converted ray encounters a second resonance (in  $k$ -space) and is transformed into a secondary converted MS ray propagating backwards to the LFS in  $x$ -space, as if it were a partial reflection of the original incoming MS wave. A new IH ray is generated by transmission in this second process and propagates mainly in  $k$ -space.

In this paper we briefly summarize the methodology and present numerical results; the theoretical derivations will be discussed in a separate paper [23]. Following the first part of the algorithm that has been developed for multiple dimensions [15], we recall that mode conversion takes place around  $\mathbf{z}_0 \equiv \mathbf{z}(\sigma_0) = (\mathbf{x}_0, \mathbf{k}_0)$ , at an orbit parameter value  $\sigma_1 \approx \sigma_0$  when the conversion monitor detects a minimum  $\mathcal{M}_{\text{con}}(\sigma_0) = 0$ . An analysis of the characteristic polynomial  $\det(\lambda \mathbf{1} - \bar{\bar{\mathbf{H}}})$  suggests that a simple conversion monitor for the reduced  $2 \times 2$  cold plasma model is the trace of the dispersion tensor (6)

$$\mathcal{M}_{\text{con}} = |\text{Tr}(\bar{\bar{\mathbf{H}}})| = |H_{11} + H_{22}|. \quad (53)$$

For the complete  $3 \times 3$  cold model, a more sophisticated monitor has to be used in the form

$$\mathcal{M}_{\text{con}} = |(H_{22}H_{33} - |H_{23}|^2) + (H_{11}H_{33} - |H_{13}|^2) + (H_{11}H_{22} - |H_{12}|^2)|. \quad (54)$$

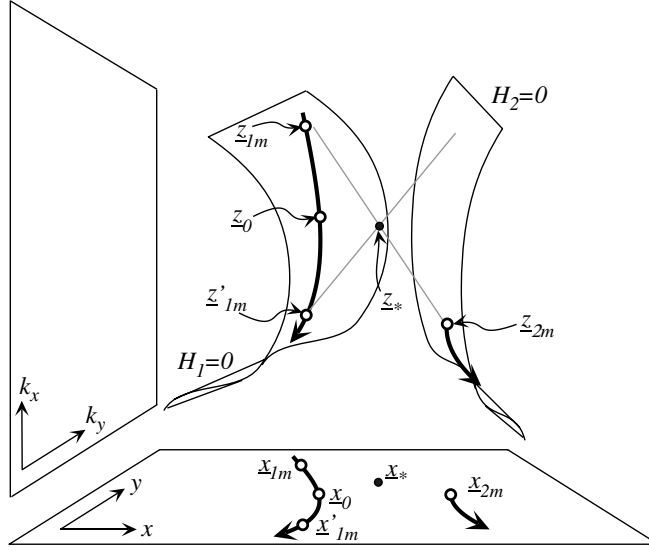


**Figure 2.** Four-dimensional phase space diagram of the mode conversion region. The simplest type of conversion involves an ‘avoided crossing’ type of geometry where two different modes satisfy the dispersion relations  $H_1 = 0$  and  $H_2 = 0$ . The rays are locally confined to a two-dimensional osculating plane and are hyperbolic with a saddle point located at  $z_*$ . When a mode conversion is first detected in the neighbourhood of  $z_0 = z(\sigma_0)$ , two ray parameters  $\sigma_{1m} < \sigma_0 < \sigma'_{1m}$  have to be determined to match the local solution with an incoming ray at  $z_{1m}$ , a converted ray at  $z'_{1m}$  and a transmitted ray at  $z_{2m}$ .

Suppose that a minimum of the conversion monitor is detected at the parameter value  $\sigma_0$ ; at this point, compute the *velocity*  $\dot{z}_0 = dz/d\sigma_1|_{\sigma_0}$  and the *acceleration*  $\ddot{z}_0 = d^2z/d\sigma_1^2|_{\sigma_0}$ . Figure 2 suggests how the velocity and the acceleration of the ray define the two basis vectors

$$\hat{e}_q = \frac{1}{\sqrt{A}}\dot{z}_0, \quad \hat{e}_p = \frac{1}{\sqrt{A}}\ddot{z}_0, \quad A = |\{\dot{z}_0, \ddot{z}_0\}| \quad (55)$$

and specify an *osculating plane* in four-dimensional phase space  $z(q, p) = z_0 + q\hat{e}_q + p\hat{e}_p$  where the incoming, the converted and the transmitted rays can locally be approximated with the legs of a hyperbola.

Up until now the eigenvalue  $H_1$  has been used as the ray Hamiltonian. It is advantageous now to switch and use the determinant of the dispersion tensor  $\det(\mathbf{H}) \equiv H(\mathbf{x}, \mathbf{k})$  as a second, alternative Hamiltonian, because it is the product of all the eigenvalues of  $\mathbf{H}$  and hence includes information from the two eigenvalues that are nearly degenerate in the conversion region. The determinant will not be used to trace rays, but only to construct the saddle structure in the conversion region, which is not possible using  $H_1$  alone.

Denote the restriction of the Hamiltonian  $H$  to the osculating plane  $H(q, p) \equiv H(z(q, p))$  and expand to second order about  $z_0$  to get  $H(z) = H(z_0) + (z - z_0) \cdot \nabla H + (z - z_0) \cdot \bar{\mathcal{H}} \cdot (z - z_0)$ . The coordinates of the saddle point, defined by the conditions  $\partial_q H = \partial_p H = 0$ , are calculated using a few Newton iterations involving the inverse of the Hessian matrix  $\bar{\mathcal{H}}$

$$z^{(n+1)} = z^{(n)} - \bar{\mathcal{H}}^{-1} \cdot \nabla H = z^{(n)} - \begin{pmatrix} \frac{\partial^2 H}{\partial q^2} & \frac{\partial^2 H}{\partial q \partial p} \\ \frac{\partial^2 H}{\partial q \partial p} & \frac{\partial^2 H}{\partial p^2} \end{pmatrix}^{-1} \cdot \begin{pmatrix} \hat{e}_q \cdot \nabla H \\ \hat{e}_p \cdot \nabla H \end{pmatrix}, \quad (56)$$

where the derivatives on the right-hand side are evaluated at  $\mathbf{z}^{(n)}$  after starting with  $\mathbf{z}^{(0)} = \mathbf{z}_0$ . This iteration converges to the saddle point  $\mathbf{z}_*$  in the osculating plane. The position of the saddle point can now be used to find initial conditions for the transmitted ray.

A matching point has to be chosen on the incoming ray. For this, backtrack from  $\mathbf{z}_0$  along the incoming trajectory to a point that is far enough away from the conversion region that the eikonal approximation is valid, but close enough that it is also possible to describe the solution with a local  $2 \times 2$  wave equation. Denote that incoming matching point with a label ‘1’ as  $\mathbf{z}_{1m} = (\mathbf{x}_{1m}, \mathbf{k}_{1m}) \equiv \mathbf{z}(\sigma_{1m})$ , where the subscript ‘m’ stands for ‘matching’ and the ray parameter  $\sigma_{1m} < \sigma_0$ . This incoming point lies on the surface  $H_1 = 0$ . A point symmetrically placed on the surface  $H_2 = 0$  can be found along the line connecting  $\mathbf{z}_{1m}$  to the saddle point  $\mathbf{z}_*$  until the line punctures the surface  $H_2 = 0$ ; this will be the initial condition for the transmitted ray. To determine its location in phase space, consider the points lying along  $\mathbf{z}(\zeta) = \mathbf{z}_{1m} + \zeta(\mathbf{z}_* - \mathbf{z}_{1m})$ . This line starts at  $\mathbf{z}_{1m}$  where  $\zeta = 0$ , passes through the saddle point  $\mathbf{z}_*$  when  $\zeta = 1$  and reaches the point that is a symmetrically placed point on the second hyperbola when  $\zeta \approx 2$ . Newton’s method can be used to hunt for the exact root of the dispersion relation  $H(\mathbf{z}(\zeta)) = 0$ . The corresponding point is finally used as the initial condition for the transmitted ray with a label ‘2’ and is denoted  $\mathbf{z}_{2m} = (\mathbf{x}_{2m}, \mathbf{k}_{2m})$ . The choice of initial conditions for the converted ray is a bit simpler, since the incoming ray smoothly connects to the converted ray. The matching point  $\sigma'_{1m} > \sigma_0$  is found along the ray with the label ‘1’, which lies past the point  $\mathbf{z}_0$  and is still in the matching region. This point is denoted  $\mathbf{z}'_{1m} = (\mathbf{x}'_{1m}, \mathbf{k}'_{1m})$ . More work is needed to define matching parameters with  $\sigma_{1m} < \sigma_0 < \sigma'_{1m}$  and to establish the accuracy of the result in different tokamak scenarios. Nonetheless, the sensitivity study shown later in section 3.1 suggests that the ray path in phase space is rather insensitive to the choice of the matching parameters, while the amplitude can vary by 20%. In order not to delay this paper, the rest of the computations will simply be performed assuming that  $\sigma_{1m} = \sigma_0 = \sigma'_{1m}$ .

It remains to determine the amplitude, the phase, the focusing tensor and the polarization of the outgoing rays. The amplitude and a first contribution to the phase are determined by the focusing tensor, which can be computed after the local  $2 \times 2$  wave equation has been put into a *normal form* (defined below) and the coupling constant has been identified. The geometrical intuition for constructing such a normal form follows from the idea that if the coupling coefficient could be set to zero, then the two different rays would intersect at the conversion point. The key is to find the ‘uncoupled’ polarizations  $\hat{\mathbf{e}}_\alpha, \hat{\mathbf{e}}_\beta$  that are approximately equal to the incoming eigenvectors in the matching region  $\hat{\mathbf{e}}_1^{(in)} \approx \hat{\mathbf{e}}_\alpha, \hat{\mathbf{e}}_2^{(in)} \approx \hat{\mathbf{e}}_\beta$ , but are constant. In other words, if the transmitted ray launched at  $\mathbf{z}_{2m}$  would be integrated backwards in the ray parameter, it would match the incoming ray of type ‘2’ with a polarization  $\hat{\mathbf{e}}_2^{(in)}$ . By analogy, the outgoing transmitted and converted rays polarizations are matched according to  $\hat{\mathbf{e}}_2^{(out)} \approx \hat{\mathbf{e}}_\alpha$  and  $\hat{\mathbf{e}}_1^{(out)} \approx \hat{\mathbf{e}}_\beta$ . The polarizations  $\hat{\mathbf{e}}_\alpha$  and  $\hat{\mathbf{e}}_\beta$  are obtained by first developing the local saddle structure and finding the asymptotes of the related hyperbolas. Along these asymptotes, it is then possible to construct the eigenvectors of the dispersion matrix.

First, Taylor-expand the  $2 \times 2$  dispersion matrix to linear order about the saddle point  $\mathbf{z}_*$ :

$$\bar{\bar{H}}(\mathbf{z}) = \bar{\bar{H}}(\mathbf{z}_*) + (\mathbf{z} - \mathbf{z}_*) \cdot \nabla_{\mathbf{z}} \bar{\bar{H}}(\mathbf{z}_*) + \dots \quad (57)$$

Far from  $\mathbf{z}_*$ , the linear term is kept as the dominant one. Now introduce a new ray Hamiltonian, which is the determinant of  $(\mathbf{z} - \mathbf{z}_*) \cdot \nabla_{\mathbf{z}} \bar{\bar{H}}(\mathbf{z}_*)$ . This new ray Hamiltonian is quadratic in  $\mathbf{z} - \mathbf{z}_*$  and is denoted as  $\bar{H}(\mathbf{z})$  to distinguish it from the full determinant of the dispersion matrix. This ray Hamiltonian generates rays via

$$\frac{d\mathbf{z}}{d\sigma} = \bar{\bar{\mathbf{J}}}_4 \cdot \nabla_{\mathbf{z}} \bar{H}. \quad (58)$$

This system of equations is *linear* in  $\mathbf{z} - \mathbf{z}_*$ , hence it can be written as

$$\frac{d\mathbf{z}}{d\sigma} = \mathbf{A} \cdot (\mathbf{z} - \mathbf{z}_*). \quad (59)$$

If the trajectories in the neighbourhood of the saddle point  $\mathbf{z}_*$  are truly hyperbolic and restricted to an osculating plane, then two real eigenvalues  $\lambda_\alpha \approx -\lambda_\beta$  will dominate the eigensystem

$$\mathbf{A} \cdot \mathbf{v}_j = \lambda_j \mathbf{v}_j, \quad j \in \{\alpha, \beta\}. \quad (60)$$

The corresponding eigenvectors  $(\mathbf{v}_\alpha, \mathbf{v}_\beta)$  define the asymptotes we seek. Along each of these two asymptotes, the linearized dispersion matrix will have a null eigenvalue. The associated polarizations are the uncoupled polarizations. Therefore, given the asymptotes  $\mathbf{v}_j$ , the *uncoupled polarizations* can be calculated using an iteration

$$\left( \mathbf{v}_j \cdot \nabla \bar{\mathbf{H}}|_{\mathbf{z}_*} \right) \hat{\mathbf{e}}_j^{(n+1)} = \hat{\mathbf{e}}_j^{(n)}, \quad j \in \{\alpha, \beta\} \quad (61)$$

starting from an arbitrary guess and keeping the unit norm  $\|\hat{\mathbf{e}}_j^{(n+1)}\| = 1$ .

At this stage, the uncoupled polarizations  $\hat{\mathbf{e}}_\alpha$  and  $\hat{\mathbf{e}}_\beta$  can be used to perform a Galerkin reduction of the dispersion matrix to construct a new  $2 \times 2$  dispersion matrix (the normal form) that involves only the two resonantly interacting modes. This matrix has diagonal entries corresponding to the *uncoupled dispersion functions*

$$H_\alpha \equiv \hat{\mathbf{e}}_\alpha^\dagger \cdot \bar{\mathbf{H}} \cdot \hat{\mathbf{e}}_\alpha, \quad H_\beta \equiv \hat{\mathbf{e}}_\beta^\dagger \cdot \bar{\mathbf{H}} \cdot \hat{\mathbf{e}}_\beta \quad (62)$$

and the off-diagonal entry representing the complex-valued coupling strength

$$\eta \equiv \hat{\mathbf{e}}_\alpha^\dagger \cdot \bar{\mathbf{H}} \cdot \hat{\mathbf{e}}_\beta. \quad (63)$$

Evaluating these quantities at the saddle point,  $H_\alpha(\mathbf{z}_*)$  and  $H_\beta(\mathbf{z}_*)$  vanish, because  $\mathbf{z}_*$  is where the two uncoupled dispersion manifolds cross. Hence, the dominant terms are linear in  $\mathbf{z}$  and define the linearized local uncoupled ray Hamiltonians  $\hat{H}_\alpha \equiv (\mathbf{a} \cdot \mathbf{x} - \mathbf{ib} \cdot \nabla) \leftrightarrow H_\alpha(\mathbf{z})$  and  $\hat{H}_\beta \equiv (\mathbf{c} \cdot \mathbf{x} - \mathbf{id} \cdot \nabla) \leftrightarrow H_\beta(\mathbf{z})$  with the standard association  $\mathbf{k} \leftrightarrow -i\nabla$ . The coupling  $\eta$  is to be evaluated at the saddle point  $\mathbf{z}_*$ . Defining the magnitude of the Poisson bracket (24) of the diagonal entries as

$$\mathcal{B} \equiv |\{H_\alpha, H_\beta\}| \quad (64)$$

the  $S$ -matrix entries can be computed and relate the incoming and outgoing field amplitudes in the  $\alpha$  and  $\beta$  channels

$$E_\alpha^{(\text{out})} = \tau(\eta) E_\alpha^{(\text{in})}, \quad E_\beta^{(\text{out})} = \beta(\eta) E_\alpha^{(\text{in})}, \quad (65)$$

$$\tau(\eta) = \exp\left(\frac{-\pi|\eta|^2}{\mathcal{B}}\right), \quad \beta(\eta) = \frac{\sqrt{2\pi\tau(\eta)}}{(\eta/\sqrt{\mathcal{B}})\Gamma(-i|\eta|^2/\mathcal{B})}. \quad (66)$$

It can be shown that unitarity of the  $S$ -matrix implies  $\tau(\eta)^2 + |\beta(\eta)|^2 = 1$ .

The eikonal phases and the focusing tensors remain to be calculated for the outgoing rays. This will now be done by matching the eikonal solution for the incoming electric field

$$\mathbf{E}_1^{(\text{in})}(\mathbf{x}(\sigma_1)) = E_1(\mathbf{x}(\sigma_1)) \exp[i\Theta_1^{(\text{in})}(\mathbf{x}(\sigma_1))]\hat{\mathbf{e}}_1(\mathbf{x}(\sigma_1)) \quad (67)$$

to an analytical solution of a local  $2 \times 2$  wave equation. This solution will then be used to find the field downstream from the conversion and to match to outgoing eikonal waves. In normal form, the local  $2 \times 2$  wave equation is

$$\begin{pmatrix} \hat{H}_\alpha & \eta \\ \eta^* & \hat{H}_\beta \end{pmatrix} \begin{pmatrix} E_\alpha(\mathbf{x}) \\ E_\beta(\mathbf{x}) \end{pmatrix} = \begin{pmatrix} \mathbf{a} \cdot \mathbf{x} - \mathbf{ib} \cdot \nabla & \eta \\ \eta^* & \mathbf{c} \cdot \mathbf{x} - \mathbf{id} \cdot \nabla \end{pmatrix} \begin{pmatrix} E_\alpha(\mathbf{x}) \\ E_\beta(\mathbf{x}) \end{pmatrix} = 0, \quad (68)$$

where the four vectors  $\mathbf{a}$ ,  $\mathbf{b}$ ,  $\mathbf{c}$ ,  $\mathbf{d}$  are identified from the Taylor series of the uncoupled Hamiltonians  $H_\alpha$  and  $H_\beta$ . The solutions of this local  $2 \times 2$  wave equation (68) are of the form

$$\mathbf{E}(\mathbf{x}) = e^{i\mathbf{k}_* \cdot (\mathbf{x} - \mathbf{x}_*)} [E_\alpha(\mathbf{x}) \hat{\mathbf{e}}_\alpha + E_\beta(\mathbf{x}) \hat{\mathbf{e}}_\beta]. \quad (69)$$

The polarizations  $\hat{\mathbf{e}}_\alpha$  and  $\hat{\mathbf{e}}_1^{(\text{in})}$  are nearly equal in the matching region for the incoming ray, so that  $E_\alpha(\mathbf{x}(\sigma_{1\text{m}}))$  can be identified from

$$E_1(\mathbf{x}(\sigma_{1\text{m}})) \exp[i\Theta_1^{(\text{in})}(\mathbf{x}(\sigma_{1\text{m}}))] = e^{i\mathbf{k}_* \cdot (\mathbf{x}(\sigma_{1\text{m}}) - \mathbf{x}_*)} E_\alpha(\mathbf{x}(\sigma_{1\text{m}})). \quad (70)$$

It is necessary now to find solutions to the local  $2 \times 2$  wave equation. The complete derivation turns out to be surprisingly complicated; details will be reported in a companion theoretical paper [23]. Here, the result is only summarized to describe how the algorithm is implemented. We first seek solutions of the *uncoupled* wave equation. Setting  $\eta = 0$  in (68), the most general solutions of the  $2 \times 2$  wave equation are linear combinations involving

$$\mathbf{E}_\alpha^{(0)}(\mathbf{x}) = e^{i\Theta_\alpha^{(0)}(\mathbf{x})} \Phi_\alpha(\mathbf{x}) \begin{pmatrix} 1 \\ 0 \end{pmatrix}, \quad \text{and} \quad \mathbf{E}_\beta^{(0)}(\mathbf{x}) = e^{i\Theta_\beta^{(0)}(\mathbf{x})} \Phi_\beta(\mathbf{x}) \begin{pmatrix} 0 \\ 1 \end{pmatrix}. \quad (71)$$

This type of solution should be valid for  $\mathbf{x}$  away from the immediate vicinity of the conversion, but still within the matching region. The complex amplitude functions  $\Phi_\alpha$  and  $\Phi_\beta$  are constant along the rays; hence they are functions of  $\mathbf{b}_\perp \cdot \mathbf{x}$  and  $\mathbf{d}_\perp \cdot \mathbf{x}$ , respectively. The perpendicular complements of  $\mathbf{b}$  and  $\mathbf{d}$  are obtained by rotation through  $90^\circ$ :  $\mathbf{b}_\perp = \bar{\mathbf{J}}_2 \cdot \mathbf{b}$ , etc. The fact that  $\Phi_\alpha$  and  $\Phi_\beta$  are constant along their respective rays is due to the fact that  $\mathbf{b}$  and  $\mathbf{d}$  are parallel to the ‘group velocities’ of the two uncoupled modes:

$$\frac{d\mathbf{x}}{d\sigma_\alpha} = -\frac{\partial H_\alpha}{\partial \mathbf{k}} = -\mathbf{b} \quad \text{and} \quad \frac{d\mathbf{x}}{d\sigma_\beta} = -\frac{\partial H_\beta}{\partial \mathbf{k}} = -\mathbf{d}. \quad (72)$$

The phase functions for the uncoupled solutions take the general form

$$\Theta_\alpha^{(0)}(\mathbf{x}) = \frac{1}{2} \frac{(\mathbf{a} \cdot \mathbf{a})(\mathbf{b} \cdot \mathbf{x})^2}{b^4} - \frac{(\mathbf{a} \cdot \mathbf{x})(\mathbf{b} \cdot \mathbf{x})}{b^2} + \frac{\lambda_\alpha}{2} (\mathbf{b}_\perp \cdot \mathbf{x})^2, \quad (73)$$

$$\Theta_\beta^{(0)}(\mathbf{x}) = \frac{1}{2} \frac{(\mathbf{c} \cdot \mathbf{d})(\mathbf{d} \cdot \mathbf{x})^2}{d^4} - \frac{(\mathbf{c} \cdot \mathbf{x})(\mathbf{d} \cdot \mathbf{x})}{d^2} + \frac{\lambda_\beta}{2} (\mathbf{d}_\perp \cdot \mathbf{x})^2. \quad (74)$$

In principle, the free parameter  $\lambda_\alpha$  can be used to match the Hessian  $\nabla \nabla \Theta_\alpha^{(0)} \equiv \mathbf{S}_\alpha$  to the Hessian of the phase of the incoming eikonal wave, i.e. the focusing tensor,  $\nabla \nabla \Theta_1(\mathbf{x}_{1\text{m}}) \equiv \mathbf{S}_1^{(\text{in})}$ . In particular:

$$\lambda_\alpha = \frac{1}{b^4} \mathbf{b}_\perp \cdot \nabla \nabla \Theta_1 \cdot \mathbf{b}_\perp. \quad (75)$$

In practice, we simply set  $\mathbf{S}_\alpha = \mathbf{S}_1^{(\text{in})}$ . This is justified because the focusing tensor is smoothly varying following the ray in regions where WKB is valid.

The parameter  $\lambda_\beta$  is determined as follows: the ray of mode  $\alpha$ ,  $(\mathbf{x}(\sigma_\alpha), \mathbf{k}(\sigma_\alpha))$  satisfies the dispersion relation for mode  $\beta$  when  $H_\beta(\mathbf{x}(\sigma_\alpha), \mathbf{k}(\sigma_\alpha)) = 0$ . For each ray of type  $\alpha$ , this occurs at one point in phase space ( $\mathbf{z}_*$ ). At this point, a ray of type  $\beta$  is launched. Hence, a family of incoming rays of type  $\alpha$  launches a family of rays of type  $\beta$  in a well-defined way. The phase  $\Theta_\beta^{(0)}(\mathbf{x})$  for the converted wave is constructed to satisfy this geometrical requirement. Again, the algebraic details are surprisingly complicated and are left to the companion theoretical paper [23]. The result is that the parameter  $\lambda_\beta$  has to be chosen as

$$\lambda_\beta = -\frac{(\mathbf{a} + \mathbf{b} \cdot \mathbf{S}_\beta^{(0)}) \cdot \mathbf{t}_c}{\mathbf{b} \cdot \mathbf{S}_\beta^{(1)} \cdot \mathbf{t}_c}, \quad \text{where} \quad \mathbf{t}_c = \bar{\mathbf{J}}_2 \cdot (\mathbf{c} + \mathbf{S}_\alpha \cdot \mathbf{d}). \quad (76)$$

Here,  $\mathbf{t}_c$  is the direction of a line, passing through  $\mathbf{x}_*$  that can be called the *line of conversion* because all neighbouring rays convert along this line. The Hessian of the transmitted ray is the same as for the incoming ray and the Hessian of the converted ray consists of two parts: one that is independent of  $\lambda_\beta$  (denoted  $\mathbf{S}_\beta^{(0)}$ ) and the other that is linear in  $\lambda_\beta$  (denoted  $\mathbf{S}_\beta^{(1)}$ )

$$\mathbf{S}_\alpha^{(\text{out})} = \mathbf{S}_\alpha^{(\text{in})}, \quad \mathbf{S}_\beta^{(\text{out})} = \mathbf{S}_\beta^{(0)} + \lambda_\beta \mathbf{S}_\beta^{(1)}, \quad (77)$$

$$\mathbf{S}_\beta^{(0)} \equiv \frac{(\mathbf{c} \cdot \mathbf{d})}{d^4} \mathbf{d} \mathbf{d}^\text{T} - \frac{1}{d^2} (\mathbf{c} \mathbf{d}^\text{T} + \mathbf{d} \mathbf{c}^\text{T}), \quad (78)$$

$$\mathbf{S}_\beta^{(1)} \equiv \mathbf{d}_\perp \mathbf{d}_\perp^\text{T}. \quad (79)$$

Together with (74), this completely determines the phase factor  $\Theta_\beta^{(0)}(\mathbf{x})$ . From the uncoupled phase factors, it is convenient to define

$$\tilde{H}_\alpha(\mathbf{x}) \equiv H_\alpha(\mathbf{x}, \nabla \Theta_\beta^{(0)}(\mathbf{x})), \quad (80)$$

$$\tilde{H}_\beta(\mathbf{x}) \equiv H_\beta(\mathbf{x}, \nabla \Theta_\alpha^{(0)}(\mathbf{x})). \quad (81)$$

These functions are linear in  $\mathbf{x} - \mathbf{x}_*$  and vanish along the line of conversion. The local solution in the channel ‘ $\alpha$ ’ can then be displayed in the matching region following the *uncoupled* ray

$$\mathbf{E}_\alpha(\mathbf{x}(\sigma_\alpha)) \approx A e^{i[\Theta_\alpha^{(0)}(\mathbf{x}(\sigma_\alpha)) - \Theta_\alpha^{(0)}(\mathbf{x}(\sigma_{1m}))]} E_\alpha^{(\text{in})}(\mathbf{x}(\sigma_{1m})) \left[ \frac{\tilde{H}_\beta(\mathbf{x}(\sigma_\alpha))}{\tilde{H}_\beta(\mathbf{x}(\sigma_{1m}))} \right]^{i|\eta|^2/B} \begin{pmatrix} 1 \\ \eta \\ \tilde{H}_\beta(\mathbf{x}(\sigma_\alpha)) \end{pmatrix}, \quad (82)$$

with  $A = 1$  for the ‘upstream’ and  $A = \tau(\eta)$  for the ‘downstream’ side of the conversion. At the matching point  $\mathbf{x}_{1m}$ , sufficiently far from the conversion so that the normalized coupling  $\eta/\tilde{H}_\beta$  becomes small, this yields

$$\mathbf{E}_\alpha(\mathbf{x}) \approx E_\alpha^{(\text{in})}(\mathbf{x}(\sigma_{1m})) \begin{pmatrix} 1 \\ \eta \\ \tilde{H}_\beta(\mathbf{x}_{1m}) \end{pmatrix} \approx E_\alpha^{(\text{in})}(\mathbf{x}(\sigma_{1m})) \begin{pmatrix} 1 \\ 0 \end{pmatrix}, \quad (83)$$

as desired. On the downstream side of conversion, insert  $\mathbf{x}_{2m}$  for  $\mathbf{x}(\sigma_\alpha)$  in the solution and use  $A = \tau(\eta)$  to get

$$\mathbf{E}_\alpha(\mathbf{x}_{2m}) \approx \tau(\eta) e^{i[\Theta_\alpha^{(0)}(\mathbf{x}_{2m}) - \Theta_\alpha^{(0)}(\mathbf{x}(\sigma_{1m}))]} E_\alpha^{(\text{in})}(\mathbf{x}(\sigma_{1m})) \left[ \frac{\tilde{H}_\beta(\mathbf{x}_{2m})}{\tilde{H}_\beta(\mathbf{x}(\sigma_{1m}))} \right]^{i|\eta|^2/B} \begin{pmatrix} 1 \\ \eta \\ \tilde{H}_\beta(\mathbf{x}_{2m}) \end{pmatrix}. \quad (84)$$

In this region, the polarizations  $\hat{\mathbf{e}}_\alpha \approx \hat{\mathbf{e}}_2^{(\text{out})}$  are nearly equal, so that the upper component of (84) multiplied by  $\exp[i\mathbf{k}_* \cdot (\mathbf{x}_{2m} - \mathbf{x}_*)]$  should be equated to the eikonal amplitude and phase functions for the transmitted wave  $E_2^{(\text{out})}(\mathbf{x}_{2m}) \exp[i\Theta_2^{(\text{out})}(\mathbf{x}_{2m})]$ , which determines them.

Following the uncoupled ray in channel  $\beta$  that was spawned by the incoming ray in channel  $\alpha$ , the matching solution for the converted rays is

$$\begin{aligned} \mathbf{E}_\beta(\mathbf{x}(\sigma_\beta)) &\approx \beta(\eta) \left( \frac{\hat{\mathbf{n}} \cdot \mathbf{v}_\alpha}{\hat{\mathbf{n}} \cdot \mathbf{v}_\beta} \right)^{1/2} e^{i[\Theta_\alpha^{(0)}(\mathbf{x}(\sigma_\beta)) - \Theta_\alpha^{(0)}(\mathbf{x}(\sigma'_{1m}))]} E_\alpha^{(\text{in})}(\mathbf{x}(\sigma'_{1m})) \\ &\times \left[ \frac{\tilde{H}_\alpha(\mathbf{x}(\sigma_\beta))}{\tilde{H}_\alpha(\mathbf{x}(\sigma'_{1m}))} \right]^{-i|\eta|^2/B} \begin{pmatrix} -\eta \\ \tilde{H}_\alpha(\mathbf{x}(\sigma_\beta)) \\ 1 \end{pmatrix}, \end{aligned} \quad (85)$$

where  $\hat{\mathbf{n}} \equiv (\mathbf{c} + S_\alpha \cdot \mathbf{d})$  is normal to the conversion line (76),  $v_\alpha = -\mathbf{b}$ ,  $v_\beta = -\mathbf{d}$  are the ‘group velocities’ of the uncoupled waves and  $\beta(\eta)$  is the conversion coefficient. Since the polarization  $\hat{\mathbf{e}}_1^{(\text{out})} \approx \hat{\mathbf{e}}_\beta$  at the matching point for the converted ray  $\mathbf{x}'_{1m} = \mathbf{x}(\sigma'_{1m})$ , this determines the outgoing converted eikonal wave: simply equate the second component in (85), multiplied by  $\exp[i\mathbf{k}_* \cdot (\mathbf{x}'_{1m} - \mathbf{x}_*)]$ , to  $E_1^{(\text{out})}(\mathbf{x}'_{1m}) \exp[i\Theta_1^{(\text{out})}(\mathbf{x}'_{1m})]$ .

In summary, the incoming eikonal ray is propagated into the matching region until a mode conversion is detected (53). The incoming ray determines the osculating plane in which the incoming, the transmitted and the converted rays are locally fitted to the legs of a hyperbola (56)–(60) in order to initialize the outgoing rays in phase space  $\mathbf{z} = (\mathbf{x}, \mathbf{k})$ . Using a first order expansion of the dispersion tensor around the saddle point  $\mathbf{z}_*$ , the uncoupled polarizations  $\hat{\mathbf{e}}_\alpha$ ,  $\hat{\mathbf{e}}_\beta$  (61) are determined together with the coupling  $\eta$  (63) and the outgoing ray amplitudes (65). Ignoring the coupling far away from the conversion region, the uncoupled ray Hamiltonians  $H_\alpha$ ,  $H_\beta$  (62) are constructed together with two functions  $\tilde{H}_\alpha$ ,  $\tilde{H}_\beta$  (80) that vanish where the mode conversion occurs. They determine the uncoupled phase functions  $\Theta_\alpha^{(0)}$ ,  $\Theta_\beta^{(0)}$  (73)–(74). The focusing tensors of the outgoing rays  $\mathcal{S} \equiv \nabla \nabla \Theta$  are then obtained by matching the far-field eikonal solutions to the local  $2 \times 2$  forms (77). The incoming eikonal wave is thus used to determine the incoming data for the local  $2 \times 2$  wave equation in channel  $\alpha$ . They determine the outgoing solutions for both channels and can be fit to outgoing rays that escape to resume an eikonal propagation.

### 3. Applications: D(20%He<sup>3</sup>) scenario in JET

A Soloviev equilibrium with parameters similar to those of a mode conversion scenario in the Joint European Torus (JET) provides for an application: major radius  $R_0 = 3.0$  m, toroidal magnetic field  $B_0 = 3.35$  T, aspect ratio  $R_0/a = 3$ , elongation  $E = 1.4$ , safety factor on axis  $q_0 = 1.5$ , two species D(20%He<sup>3</sup>) plasma with  $n_{0,D} = 5.6 \times 10^{19} \text{ m}^{-3}$ ,  $n_{0,\text{He}3} = 1.4 \times 10^{19} \text{ m}^{-3}$  and parabolic profiles obtained using the parameters  $c = d = 1$  in equation (2). The antenna frequency is set to 37 MHz so as to match the IH frequency on the high magnetic field side (HFS) of the magnetic axis. For simplicity, we use the reduced  $2 \times 2$  cold plasma model and keep one single toroidal wave-vector component  $k_{\varphi,\text{ant}} = -4.67 \text{ m}^{-1}$  that is dominant in the antenna spectrum.

#### 3.1. Validation in the tokamak mid-plane

Choosing initial conditions so as to confine the ray trajectories in the tokamak mid-plane ( $Z \simeq 0$ ), the complete toroidal problem involves one dominant spatial dimension and becomes similar to the well-known Budden problem [24].

Figure 3 suggests how a MS ray is initialized on the LFS of the torus at  $R = 3.5$  m with a wave-vector  $k_R = -27 \text{ m}^{-1}$  (label 1, blue curve,  $t = 0$ ). Starting the integration forward in time, the Hamilton equations (21)–(22) are evolved until the monitor  $\dot{\mathcal{M}}_{\text{con}} = 0$  (53) signals that a mode conversion takes place (label 2 at  $t = 0.26 \mu\text{s}$ ). Invoking the conversion algorithm (55)–(56) the incident ray ( $R = 2.52$  m,  $k_R = -11 \text{ m}^{-1}$ ) is split into a converted ( $R = 2.52$  m,  $k_R = -11 \text{ m}^{-1}$ ) and a transmitted MS ray ( $R = 2.48$  m,  $k_R = -27 \text{ m}^{-1}$ ) on the HFS of the IH layer (label 2', green curve). After the conversion, the integration proceeds with two rays: the converted ray stays around  $R = 2.52$  m as it undergoes a reflection (label 3) and the transmitted MS ray propagates to the low density cutoff at  $R = 2.11$  m where it is also reflected (label 3' at  $t = 0.32 \mu\text{s}$ ). Stepping forward in time after point 3, a new mode conversion is detected (label 4 at  $t = 0.52 \mu\text{s}$ ) and generates a new converted MS ray ( $R = 2.52$  m,  $k_R = 11 \text{ m}^{-1}$ ) and a transmitted IH ray ( $R = 3.07$  m,  $k_R = 27 \text{ m}^{-1}$ ) that propagates with increasingly short

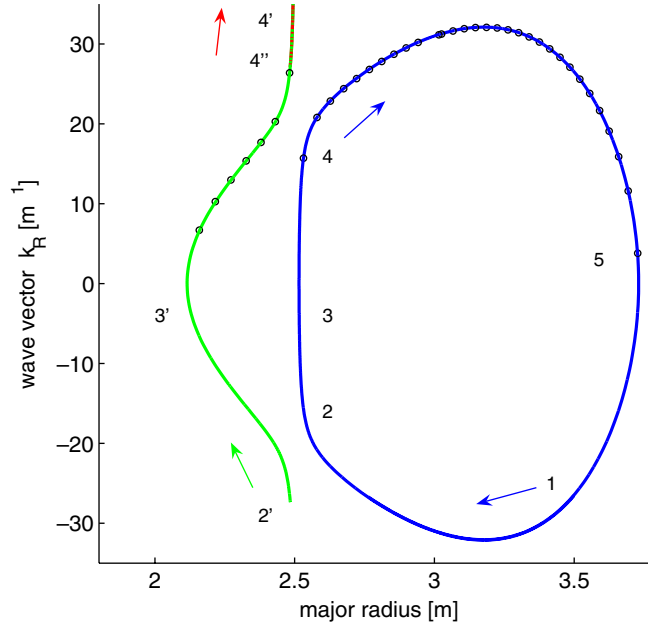


**Figure 3.** Validation with a D(20%He<sup>3</sup>) mode conversion scenario in the mid-plane of the JET, showing a comparison between solutions of the local dispersion relation  $H(R, k_R) = 0$  (black dot, ●) and the ray trajectories  $(R(\sigma), k_R(\sigma))$ . The MS ray launched on the LFS bounces between the IH layer and the plasma edge (ellipsoid on the right, 1–5 in blue). Mode conversion successively generates a transmitted MS ray on the HFS (2' in green) and a transmitted IH ray (4'' in red), which overlap and interfere for large values of  $k_R$ .

wavelength (label 4'', red curve hard to distinguish on the plot). On the LFS of the IH layer, the MS ray resumes its propagation outwards and is eventually reflected at the low density cutoff around  $R = 3.73$  m (label 5,  $t = 0.80 \mu\text{s}$ ) before it turns back towards the IH layer. For an additional consistency check, figure 3 shows that the ray trajectories in phase space coincide with small circles that depict a discrete set of solutions of the dispersion relation  $H_\alpha(R, Z = 0, k_R, k_Z = 0) = 0$ . The hyperbolic nature of the ray trajectories is clearly visible in the neighbourhood where mode conversion takes place.

The same study with the ray confined near the tokamak mid-plane is reproduced in figure 4 to show the evolution of the phase space coordinates  $(R, k_R)$  in parallel with some elements of the focusing tensor ( $\partial_{RR}\Theta$  and  $\partial_{ZZ}\Theta$ ,  $\partial_{RZ}\Theta$  is not shown), the eikonal amplitude  $E$  and the eikonal phase  $\Theta$ . Starting with a weak focusing when the MS ray (in blue) is launched  $\partial_{RR}\Theta = 41 \text{ m}^{-2}$ , the amplitude first reproduces the  $E \propto 1/\sqrt{|k_R|}$  dependence due to refraction in a nonuniform plasma until the first mode conversion takes place at  $t = 0.26 \mu\text{s}$ . The transmission coefficient (66)  $\tau_{\text{MS}} = 0.27$  and the amplitude  $|E|$  of the transmitted MS ray (in green) are large, which is consistent with the weak coupling (63)  $|\eta|^2/\mathcal{B} = 0.41$  that is expected in this D(20%He<sup>3</sup>) scenario.

Maslov transformations (48), (52) have been carried out to avoid caustics between  $t = 0.26\text{--}0.32 \mu\text{s}$  for the incoming MS ray and  $t = 0.35\text{--}0.36 \mu\text{s}$  for the transmitted MS ray. Each change in representation between  $x$ - and  $k$ -space appears as a discontinuity in figure 4—displaying only the values when the integration is performed in  $x$ -space and setting the plotted curve artificially to zero when the evolution is carried out in  $k$ -space. In fact, the evolution of the integration variables is smooth in both  $x$ - and  $k$ -space and the end result does not depend

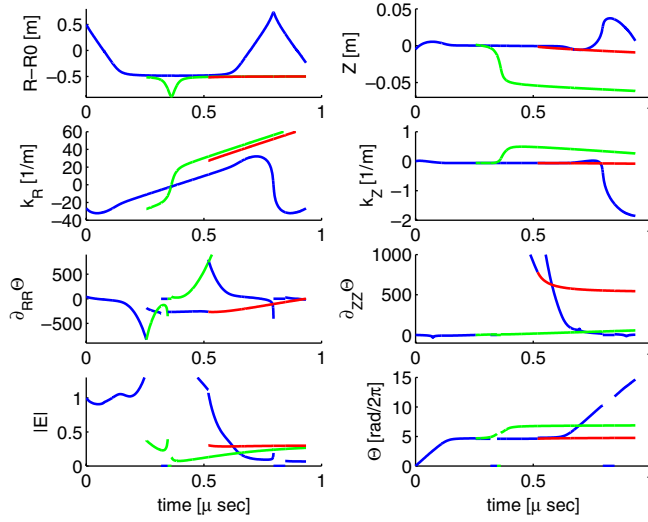


**Figure 4.** Same study as in figure 3, showing the time evolution of the phase space variables ( $x, k$ ), the elements of the focusing tensor ( $\nabla\nabla\Theta$ ), the amplitude  $E$  and the phase  $\Theta$  of the eikonal waves.

on the exact matching time when the Maslov transformations are carried out provided they are sufficiently far away from the caustics. The second mode conversion at  $t = 0.52 \mu\text{s}$  is equally effective and yields exactly the same value of transmission to the IH ray (in red) with  $\tau_{\text{IH}} = 0.27$ . This symmetry between the two conversions is indeed expected in the tokamak mid-plane and provides for another self-consistency check. The eikonal amplitude of the MS ray on the LFS of the IH layer drops considerably during the time interval  $t = 0.52\text{--}0.6 \mu\text{s}$ : a closer look shows that the MS ray suffers from strong defocusing in the vertical direction  $\partial_{ZZ}\Theta = 2000\text{--}500 \text{ m}^{-2}$  immediately after mode conversion takes place. At present, it is not clear whether this effect is physical (e.g. the shape of the MS wave evanescent layer that is indeed thicker on the tokamak mid-plane than above/below) or if it is due to a bad matching as a consequence of a naive choice of the ray parameters  $\sigma_{1\text{m}} = \sigma_0 = \sigma'_{1\text{m}}$ .

To assess the sensitivity of choosing adequate matching parameters, figure 5 shows how selected quantities deviate from the values obtained with the naive choice  $t_{1\text{m}} = t_0 = t'_{1\text{m}}$ , where the matching times coincide with the time when the mode conversion is detected. The iteration (56) converges to nearly the same saddle point  $z_*$  independently of the incoming ray  $z_{1\text{m}}$ , so that the coupling  $\eta(z_*)$  (63) and the transmission  $\tau(z_*)$  (66) do not depend much on the matching time. This can be put in contrast with the transmission evaluated along the ray  $\tau(z_{1\text{m}})$ , which depends on the incoming polarizations and varies far more quickly. A small 1% deviation in the position of the incoming ray  $R_{1\text{m}}$  when the matching is performed early affects the transmitted ray  $R_{2\text{m}}$  by the same amount; the same level of accuracy is also found for the converted ray  $R'_{1\text{m}}$ . Despite a clearly defined saddle, different matching times  $t_{1\text{m}} < t_0$  do affect the incoming amplitude  $E_{1\text{m}}$  as it grows towards a caustic around  $t = 0.3 \mu\text{s}$  in figure 4. More work is required to properly attribute the incoming amplitude and reduce the uncertainty for the transmitted  $E_{2\text{m}}$  and converted  $E'_{1\text{m}}$  that is now around 20%.

Finally, note that by piecing together eikonal waves across a conversion region where the local solution is known analytically, no singular behaviour of the electric field is ever encountered. This is in contrast to full-wave methods, where singularities appear if a reduced  $2 \times 2$  model (7) is used without dissipation.

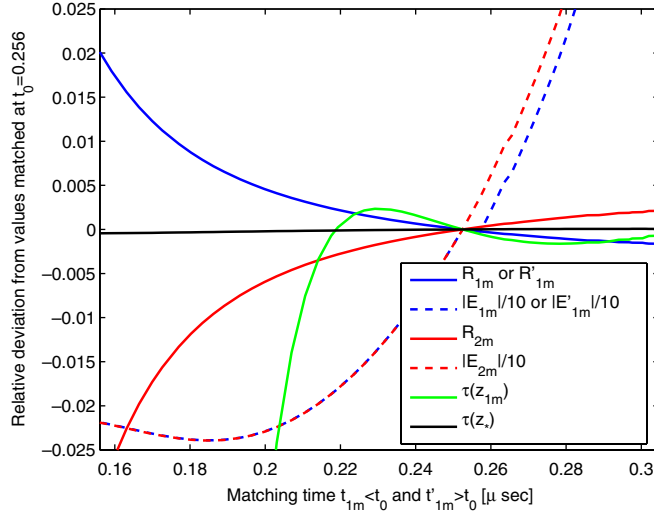


**Figure 5.** Sensitivity study for the matching at the first mode conversion in figure 3 (labels 2 and 2') detected at  $t_0 = 0.256 \mu\text{s}$ . The figure shows how selected quantities depend on the choice of the matching times  $t_{1m} < t_0 < t'_{1m}$ , when the incoming and the outgoing rays are matched to the analytical solution. The relative deviation from values obtained at  $t_0$  is displayed as a function of  $t_{1m}$  on the left ( $t_{1m} < t_0$ ), and as a function of  $t'_{1m}$  on the right  $t_0 < t'_{1m}$  as appropriate.

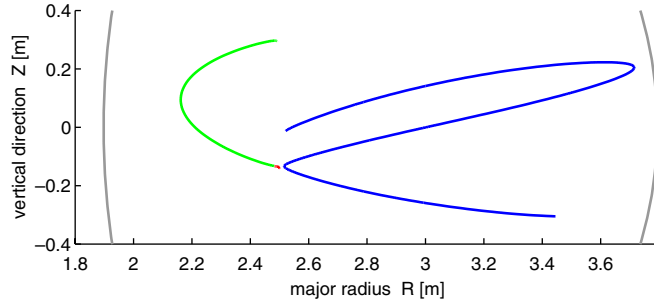


**Figure 6.** Toroidal mode conversion in the cross-section of JET using the same D(20%He<sup>3</sup>) scenario as in figure 3. The figure shows the trajectory of an incoming MS ray (blue, right), a transmitted MS ray (green, left) and a transmitted IH wave (red, barely visible). The plasma boundaries appear on each side of the figure (grey).

### 3.2. Mode conversion away from the mid-plane

Extending the study away from the tokamak mid-plane, figures 6 and 7 show the evolution of a ray starting from  $(R, Z) = (3.45, -0.31) \text{ m}$  with a wave-vector  $k_R = -27 \text{ m}^{-1}$  that is first purely horizontal  $k_Z = 0 \text{ m}^{-1}$ . Refraction from the higher density in the core rapidly leads to an increase of  $k_Z = 0 \rightarrow 6.8 \text{ m}^{-1}$ , so that the incoming MS ray points upwards when it spawns transmitted MS and IH rays at  $t = 0.27$  and  $0.48 \mu\text{s}$ . Because of the toroidal nature of the mode conversion, the transmission coefficients are not anymore equal with  $\tau_{\text{MS}} = 0.25$  for the first and  $\tau_{\text{IH}} = 0.28$  for the second mode conversion. The rest of the evolution is qualitatively similar to the description given in the previous section; nevertheless, because of the vertical

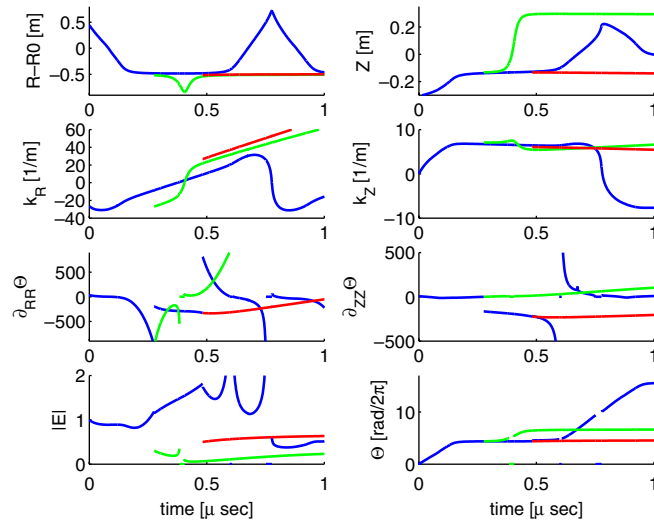


Figure 7. Same study as in figure 6, showing the time evolution of the variables.

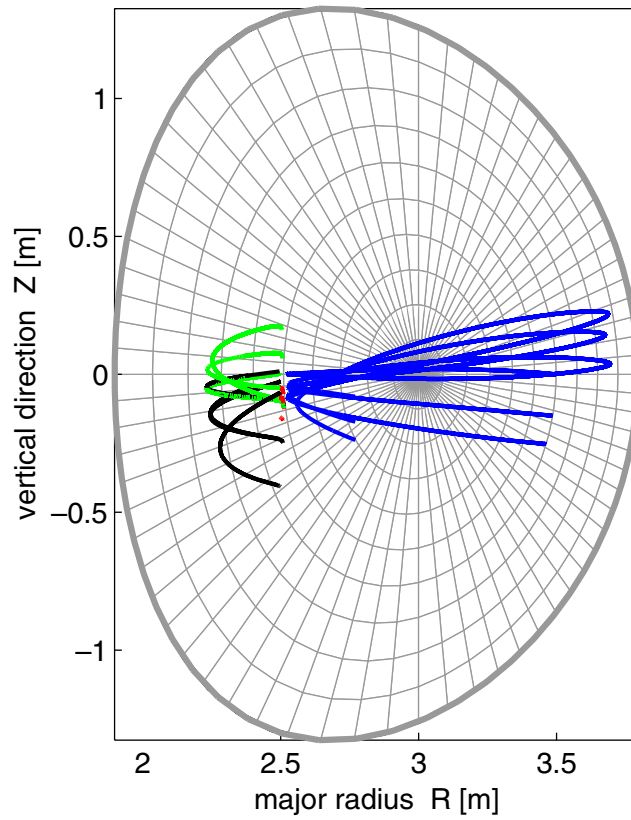
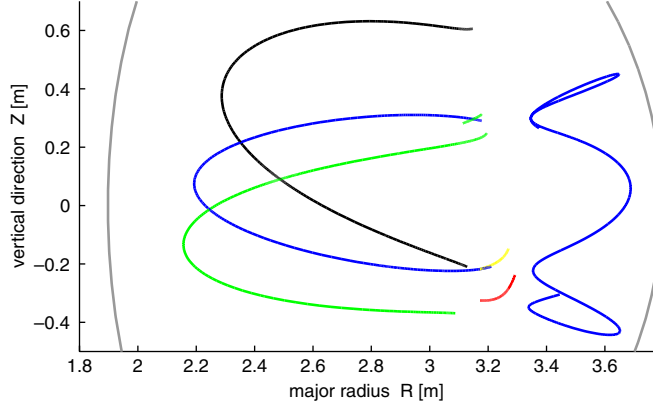


Figure 8. Trajectory of three rays in the cross-section of JET using the same parameters as in figure 3 to reproduce a D(20%He<sup>3</sup>) mode conversion in a 'hybrid scenario'.



**Figure 9.** Trajectories spawned by a single MS ray in a D(20%H) scenario.

spreading of the rays above/below the tokamak mid-plane, it is clear that the radial deposition of power could be significantly different.

### 3.3. Modelling of an experiment in JET

Repeating the same calculation with a number of rays, it is possible to simulate the propagation of the electromagnetic field excited by the ICRF antenna in a mode conversion scenario on JET; figure 8 shows how three MS rays propagate back and forth across the plasma, bouncing twice against the mode conversion layer to spawn  $3 \times 2 = 6$  pairs of transmitted MS and IH rays. Superposing all the trajectories onto a grid with surfaces of constant poloidal magnetic flux  $s = 0, 0.1, 0.2$ , etc, figure 8 shows that most of the mode converted power is deposited around  $R = 2.6$  m in a rather narrow region of the minor radius  $s \simeq [0.45-0.55]$ . Since the transmitted rays propagate far from the cyclotron resonances at  $R_D \simeq 2.09$  and  $R_{\text{He}3} \simeq 2.78$  m, the converted power should entirely be deposited on the electrons via Landau damping when  $k_{\parallel}$  becomes sufficiently large. Of course, a comparison between experimental data and the simulation requires detailed knowledge of the power deposition profiles and goes beyond the scope of this paper; nevertheless, it appears that the ray-tracing calculations are at least in qualitative agreement with experiments that have been carried out in JET.

## 4. Results: D(20%H) scenario

In this section we test the mode conversion algorithm in a case with strong coupling, when the evanescent region in front of the IH layer is large and the transmission coefficient is small. This is achieved by replacing helium with hydrogen and reducing the toroidal magnetic field  $B_0 = 3.0$  T so as to move the IH layer to the LFS of the torus. Keeping the rest of the parameters the same as in section 3, figures 9 and 10 show how a single ray (in blue) starts below the mid-plane and first propagates down/inwards to spawn a pair of transmitted MS (green) and IH rays (red) when  $t = 0.3 \mu\text{s}$ . The couplings for both conversions (63)  $|\eta|^2/B = 7.0, 5.2$  yield transmissions  $\tau < 10^{-7}$  that are negligibly small. Pursuing the calculation only to study the ray dynamics, the MS ray bounces back and forth between the low density cutoff and the conversion layer and spawns new pairs of transmitted MS and IH rays (black, yellow) with  $|\eta|^2/B = 6.7, 4.8$  around  $t = 1.1 \mu\text{s}$  and (blue and green) with  $|\eta|^2/B = 4.6, 6.7$  around  $t = 1.8 \mu\text{s}$ . A closer look at the trajectories in figure 9 shows that the initial positions of the

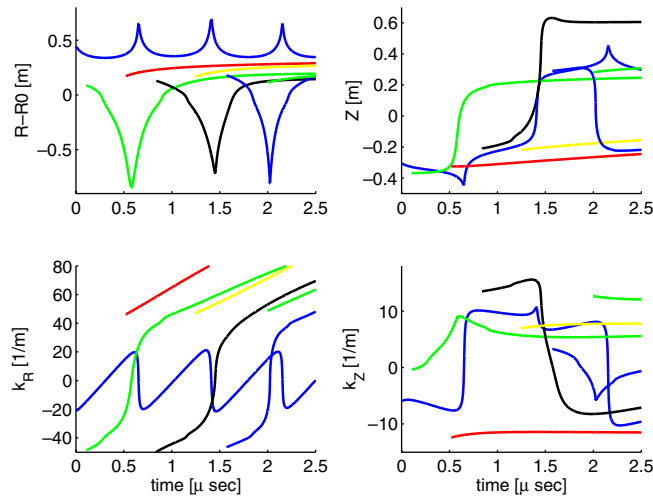


**Figure 10.** Same study as in figure 9, showing the time evolution of the variables.

transmitted rays approximatively form a line that tilts clockwise away from the vertical for the MS rays and counter-clockwise for the IH ray. This breaking of the symmetry is due to the poloidal magnetic field induced by the plasma current and has also been observed in full-wave calculations [6]. It is finally worth mentioning that with a  $2 \times 2$  cold plasma model, the IH rays can propagate a significant distance in the cross-section of the tokamak, starting towards the LFS of the torus and bending up or down because of the poloidal field.

## 5. Conclusions

A new ray-tracing code has been developed that accounts for multidimensional mode conversion and caustics in a realistic tokamak geometry. Individual rays evolve in phase space and are supplemented by the focusing tensor, the eikonal amplitude and phase to describe the transport of electromagnetic power along the ray trajectory. The first version of the RAYCON code concentrates on the ion cyclotron range of frequencies and uses a cold plasma model to simulate an IH mode conversion scenario in JET.

Important future extensions of this code would be to include kinetic effects to treat absorption of the rays via Landau damping and three-dimensional equilibria for stellarators. Appropriate modification of the dispersion tensor to include the electron dynamics will also make it possible to treat mode conversion in the ECRF.

## Acknowledgments

The implementation has been tested in limiting cases in the form of student projects involving O Mischchenko, A Atle and J Höök. AJ thanks the Berkeley group for their hospitality and support, without which the development of the RAYCON code would not have been possible; his work was partly covered by faculty funding, *secondement* to the EFDA-JET work programme and sponsoring from [www.lifelong-learners.com](http://www.lifelong-learners.com). ET and AK were supported by the NSF-DOE Partnership in Basic Plasma Physics and the US-DOE Office of Fusion Energy Sciences.

### Appendix. Local field in the vicinity of a caustic

Having determined  $\tilde{E}(\mathbf{k})$  and  $\tilde{\Theta}(\mathbf{k})$  by ray methods, it is necessary to calculate  $E(\mathbf{x})$  in the caustic region:

$$E(\mathbf{x}) = \int \frac{d^2k}{(2\pi)^2} e^{i\mathbf{k}\cdot\mathbf{x}} \tilde{E}(\mathbf{k}) = \int \frac{d^2k}{(2\pi)^2} e^{i\mathbf{k}\cdot\mathbf{x}} e^{i\tilde{\Theta}(\mathbf{k})} \tilde{E}(\mathbf{k}) \hat{e}(\mathbf{x}_0(\mathbf{k}), \mathbf{k}). \quad (86)$$

Monitor  $\det(\nabla_k \nabla_k \tilde{\Theta})$  along the ray and define the caustic point  $(\mathbf{x}_0, \mathbf{k}_0)$  where the monitor passes through zero. Obtain the principal axes of  $\nabla_k \nabla_k \tilde{\Theta}$ . Let  $(x', y')$  be the coordinates aligned with these axes (with  $\mathbf{x}' = 0$  at  $\mathbf{x}_0$ ) so that

$$\frac{\partial^2 \tilde{\Theta}}{\partial k_{x'}^2} = 0, \quad \text{and} \quad \frac{\partial^2 \tilde{\Theta}}{\partial k_{y'}^2} \neq 0. \quad (87)$$

Expand  $\tilde{\Theta}(\mathbf{k})$  about  $\mathbf{k}_0$  and include the first leading terms beyond linear order:

$$\tilde{\Theta}(\mathbf{k}) = \tilde{\Theta}(\mathbf{k}_0) + \mathbf{k}' \cdot \left. \frac{\partial \tilde{\Theta}}{\partial \mathbf{k}'} \right|_{\mathbf{k}_0} + \frac{1}{2} k_{y'}^2 \left. \frac{\partial^2 \tilde{\Theta}}{\partial k_{y'}^2} \right|_{\mathbf{k}_0} + \frac{1}{3!} k_{x'}^3 \left. \frac{\partial^3 \tilde{\Theta}}{\partial k_{x'}^3} \right|_{\mathbf{k}_0} + \dots \quad (88)$$

Therefore,

$$E(\mathbf{x}) \approx \tilde{E}(\mathbf{k}(\mathbf{x})) \int \frac{d^2k}{(2\pi)^2} e^{i(\mathbf{k}_0 + \mathbf{k}') \cdot (\mathbf{x}_0 + \mathbf{x}')} e^{i[\tilde{\Theta}(\mathbf{k}_0) - \mathbf{k}_0 \cdot \mathbf{x}_0 - \mathbf{k}' \cdot \mathbf{x}_0]} e^{i \left[ \frac{1}{2} k_{y'}^2 \left. \frac{\partial^2 \tilde{\Theta}}{\partial k_{y'}^2} \right|_{\mathbf{k}_0} + \frac{1}{3!} k_{x'}^3 \left. \frac{\partial^3 \tilde{\Theta}}{\partial k_{x'}^3} \right|_{\mathbf{k}_0} \right]}. \quad (89)$$

This becomes

$$E(\mathbf{x}) \approx \tilde{E}(\mathbf{k}(\mathbf{x})) e^{i[\tilde{\Theta}(\mathbf{k}_0) - \mathbf{k}_0 \cdot (\mathbf{x} - \mathbf{x}_0)]} \int \frac{dk_{x'}}{(2\pi)} e^{ik_{x'}x' + \frac{1}{6} k_{x'}^3 \left. \frac{\partial^3 \tilde{\Theta}}{\partial k_{x'}^3} \right|_{\mathbf{k}_0}} \int \frac{dk_{y'}}{(2\pi)} e^{i[k_{y'}y' + \frac{1}{2} k_{y'}^2 \left. \frac{\partial^2 \tilde{\Theta}}{\partial k_{y'}^2} \right|_{\mathbf{k}_0}]}. \quad (90)$$

The integration over  $k_{y'}$  is of the Gaussian type, while that over  $k_{x'}$  of the Airy type:

$$E(\mathbf{x}) = \tilde{E}(\mathbf{k}(\mathbf{x})) e^{i[\tilde{\Theta}(\mathbf{k}_0) + \mathbf{k}_0 \cdot \mathbf{x}']} \left[ \frac{1}{\pi} \int_0^\infty dt \cos(x't + at^3) \right] \times \left[ \frac{1}{\sqrt{2\pi}} e^{i(\pi/4)} \left( \frac{\partial^2 \tilde{\Theta}}{\partial k_{y'}^2} \right)^{-1/2} e^{i(y'^2/2) \partial k_{y'}/\partial y'} \right], \quad (91)$$

where  $t \equiv k_{x'}$  and  $a \equiv \frac{1}{6} (\partial^3 \tilde{\Theta} / \partial k_{x'}^3)$ . The Airy integral gives

$$\frac{1}{\pi} \int_0^\infty dt \cos(x't + at^3) = \begin{cases} \frac{1}{(3a)^{1/3}} \text{Ai} \left( \frac{x'}{(3a)^{1/3}} \right), & a > 0, \\ \frac{1}{(3|a|)^{1/3}} \text{Ai} \left( -\frac{x'}{(3|a|)^{1/3}} \right), & a < 0. \end{cases} \quad (92)$$

In summary, equation (91) provides a local solution in the vicinity of a caustic.

### References

- [1] Villard L, Brunner S and Vaclavik J 1995 *Nucl. Fusion* **35** 1173  
Villard L, Appert K, Gruber R and Vaclavik J 1986 *Comput. Phys. Rep.* **4** 95
- [2] Bécoulet A *et al* 1994 *Phys. Plasmas* **1** 2908
- [3] Fukuyama A *et al* 1998 *Proc. 17th Fusion Energy Conf. (Yokohama)* IAEA-CN-69/THP2  
Fukuyama A *et al* 1986 *Comput. Phys. Rep.* **4** 137
- [4] Jaun A, Appert K, Vaclavik J and Villard L 1995 *Comput. Phys. Commun.* **92** 153  
Jaun A, Blomqvist K, Bondeson A and Rylander T 2001 *Comput. Phys. Commun.* **135** 74

- 
- [5] Brambilla M 1999 *Plasma Phys. Control. Fusion* **41** 1  
Brambilla M and Krücken T 1988 *Nucl. Fusion* **28** 1813
- [6] Jaeger E F, Berry L A, Azevedo E D', Batchelor D B and Carter M D 2001 *Phys. Plasmas* **8** 1573
- [7] LinLiu Y R *et al* 1999 *26th EPS Conf. Controlled. Fusion and Plasmas Physics (Maastricht, 14–18 June)* vol 23J (ECA) 1245  
Batchelor D B and Goldfinger R C 1980 *Nucl. Fusion* **20** 403
- [8] Smirnov A P and Harvey R W 1995 *Bull. Am. Phys. Soc.* **40** 1837
- [9] Brambilla M and Cardinali A 1982 *Plasma Phys.* **24** 1187  
Brambilla M 1986 *Comput. Phys. Rep.* **4** 71
- [10] Keller J B and Rubinow S I 1960 *Ann. Phys.* **9** 24
- [11] Jaun A, Hellsten T and Chiu S C 1998 *Nucl. Fusion* **38** 153
- [12] Jaeger E F *et al* 2003 *Phys. Rev. Lett.* **90** 195001
- [13] Nelson-Melby E *et al* 2003 *Phys. Rev. Lett.* **90** 155004
- [14] Batchelor D B *et al* 2005 *Phys. Today* **2** 35
- [15] Tracy E R, Kaufman A N and Jaun A 2001 *Phys. Lett. A* **290** 309
- [16] Stix T H 1992 *Waves in Plasmas* (New York: American Institute of Physics)
- [17] Kaufman A N 1991 Phase-space action principles, linear mode conversion, and the generalized Fourier transformation *Nonlinear and Chaotic Phenomena in Plasmas, Fluids and Solids* ed W Rozmus and J A Tuszynski (New Jersey, USA: World Scientific)
- [18] Tracy E R, Kaufman A N and Brizard A J 2003 *Phys. Plasmas* **10** 2147
- [19] Kaufman A N, Ye H and Hui Y 1987 *Phys. Lett. A* **120** 327
- [20] Bracher C and Delos J B 2006 *Phys. Rev. Lett.* **96** 100404-1
- [21] Tracy E R and Kaufman A N 2003 *Phys. Rev. Lett.* **91** 130402
- [22] Kaufman A N, Tracy E R and Brizard A J 2005 *Phys. Plasmas* **12** 022101
- [23] Tracy E R, Kaufman A N and Jaun A Local fields for asymptotic matching in multidimensional mode conversion, in preparation
- [24] Budden K 1961 *Radio Waves in the Ionosphere* (Cambridge: Cambridge University Press)